and Myc (4). These iPS factors are thought to reprogram somatic nuclei in a somewhat similar way as ooplasm does in reconstructed oocytes by nuclear transfer (NT). However, with the exception of Oct4, these factors are not highly expressed maternally in oocytes, and only increased by zygotic transcription during preimplantation, based on expression sequence tag (EST) frequencies in Unigene cDNA libraries and microarray data from oogenesis to preimplantation development (5). Although pluripotency is achieved within 2 days in NT embryos reconstructed with a somatic nucleus, it takes approximately 2 weeks for the establishment of iPS cells. Such immediate induction of pluripotency during preimplantation development is attributed to well-organized transcriptional regulation, i.e. waves of transcription whereby maternal gene products trigger ZGA, which in turn fuels MGA. On the other hand, the forced simultaneous transcription of iPS factors in somatic cells does not efficiently induce these waves of transcription, and it takes a long time to activate the other genes necessary for pluripotency. Studying transcriptional regulation during preimplantation development would therefore also help unravel the establishment of iPS cells as well as pluripotency in these cells.

Large-scale EST projects (6–8) and DNA microarray studies (3,9–11) have revealed many novel genes zygotically expressed during preimplantation development. Very few of these genes, however, are exclusively expressed in preimplantation embryos (12), and such genes ought to have important roles during preimplantation development. For example, *Zscan4*, a novel transcription factor, is expressed specifically in 2-cell stage embryos and a subset of ES cells (13). Reduction of *Zscan4* transcript levels by siRNAs delays progression from the 2-cell to the 4-cell stage, and produces blastocysts that neither implant *in vivo* nor proliferate in blastocyst outgrowth culture. Thus, a transcription factor expressed exclusively in preimplantation embryos is potentially a key regulator of global gene expression changes during preimplantation development. On the other hand, reprogramming gene expression during ZGA and MGA requires considerable changes in chromatin structure (14–16), and modulation of chromatin folding affects access of regulatory factors to their cognate DNA-binding sites. This modulation can be achieved by loosening the chromatin structure, by disrupting the nucleosome structure, by DNA bending and unwinding, and by affecting the strength of DNA-histone interactions via postsynthetic modifications of histones (17,18). Many of these structural changes are mediated by a large and diverse superfamily of high-mobility-group (HMG) proteins, which are the second most abundant chromosomal proteins after histones (18).

This study identified a novel preimplantation-specific gene, *Hmgpi*, which encodes a chromosomal protein containing HMG box domains. It reports a detailed expression analysis of *Hmgpi* and the *Hmgpi*-encoded protein (HMGPI), which was translocated from the cytoplasm to nuclei at the blastocyst stage. Loss-of-function studies were also conducted using siRNA technology. The siRNA-induced reduction in *Hmgpi* expression caused developmental loss at preimplantation stages and hampered implantation through reduced proliferation of both ICM-derived cells and trophectodermal cells during peri-implantation development.

## RESULTS

### Gene structure of a preimplantation-stage-specific gene, *Hmgpi*

*In silico* analysis identified *Hmgpi* (an **HMG**-box protein, **p**reimplantation-embryo-specific) as a preimplantation-stage-specific gene encoding a chromosomal protein containing HMG box domains. The *Hmgpi* transcript levels are probably upregulated during ZGA (1- to 2-cell stages) to peak at the 4-cell stage, based on gene expression profiling (3,9) (Fig. 1A). Using the public expressed-sequence tag (EST) database, 16 cDNA clones were found exclusively in preimplantation-embryo libraries (2- to 8-cell stages) (Fig. 1B). One of these contained the full *Hmgpi* gene coding sequence (AK163257) (Fig. 1C), spanning 2579 bp and split into two exons, which encode a protein of 394 amino acids (aa) (NP_001028965) harboring a SANT domain ('SWI3, ADA2, N-CoR, and TFIIIB' DNA-binding domain) and two HMG-box domains, based on SMART domain prediction analysis (19) (Fig. 1C). In the NCBI Gene database, the *Hmgpi* gene is called Ubtf-like 1 (*Ubtfl1*) based on aa sequence similarity (36% identity and 58% positives by BLAST) to *Ubtf*-encoded protein 'upstream binding transcription factor', which contains a SANT domain and six HMG-box domains. Two rat homologs (*Ubtfl1* and *RGD1304745*) and three human homologs (*UBTFL1-3*) of the mouse *Hmgpi* were identified by BLASTing of NP_001028965 against the NCBI nucleotide database. Pairwise alignment scores by BLAST of amino acid sequences for rat and human homologs are 72.3–72.5% and 53.8–54.1%, respectively (Fig. 1D and Supplementary Material, Table S1), while those for nucleotide sequences are 83.7 and 66.8–67.0%, respectively. All these human homologs were predicted by *in silico* genome-based analysis, and have no ESTs in the Unigene database. The absence of human ESTs may reflect the paucity of cDNA libraries of human preimplantation embryos in the Unigene database, despite specific expression of the Hmgpi gene in human preimplantation embryos. Based on the number and the type of HMG-box domains, this novel protein could also be categorized into the HMG-box family (HMGB). A dendrogram of aa sequence similarity in HMG family proteins indicates two HMG subgroups (Fig. 1E). One includes the HMG-nucleosome binding family (HMGN) and the HMG-AT-hook family (HMGA), and the other is HMGB that includes HMGPI. All members of HMGB contain two HMG-box domains ('HMG-box' or 'HMG-UBF_HMG-box').

### Expression of the *Hmgpi* gene and protein

First, we experimentally confirmed the preimplantaion-stage-specific expression pattern of *Hmgpi* suggested by the *in silico* analysis. Northern blot analysis using a mouse multiple tissue poly(A)RNA panel (FirstChoice® Mouse Blot 1 from Ambion, Austin, TX, USA) failed to detect expression of the *Hmgpi* gene (data not shown). While RT–PCR analysis using cDNA isolated from mouse adult tissues and fetuses (E7, E11, E15 and E17) also failed to show *Hmgpi* expression, RT–PCR analysis for preimplantation embryos indicated *Hmgpi* expression from the 2-cell embryo to the blastocyst

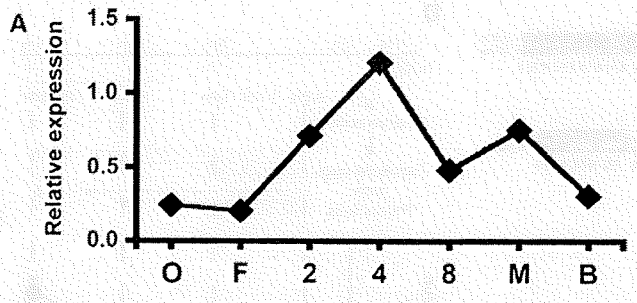


B

| Developmental stage | Gene EST | Total EST in pool |
|---|---|---|
| Oocyte | 0 | 19488 |
| Unfertilized ovum | 0 | 20366 |
| Zygote | 0 | 26382 |
| Cleavage | 16 | 65852 |
| Blastocyst | 0 | 69938 |
| Egg cylinder | 0 | 12257 |
| Gastrula | 0 | 28673 |
| Organogenesis | 0 | 128591 |
| Fetus | 0 | 670244 |
| Neonate | 0 | 107177 |
| Juvenile | 0 | 293396 |
| Adult | 0 | 1026072 |

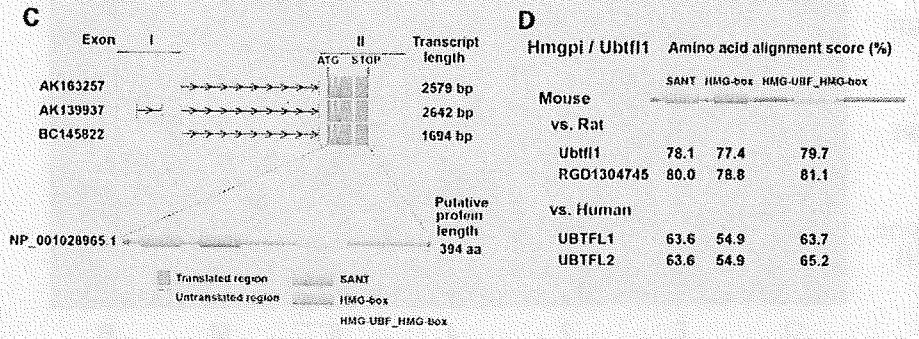


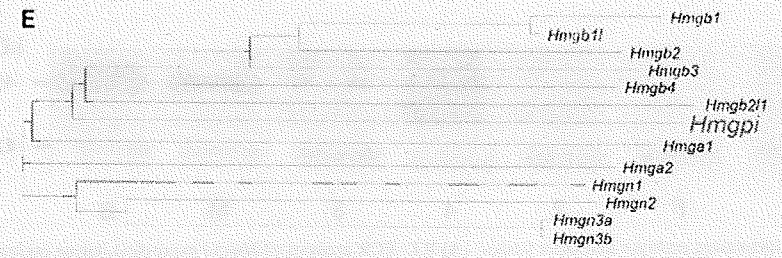


**Figure 1.** *In silico* analysis of *Hmgpi* expression. (**A**) Previous microarray analysis of *Hmgpi* expression. *Hmgpi* expression appeared at the 2-cell stage, peaked at the 4-cell stage and then decreased (3). (**B**) Expression sequence tag (EST) frequencies in Unigene cDNA libraries. Out of 4.7 million mouse ESTs, 16 *Hmgpi* clones were exclusively detected at the cleavage stages: 9, 2 and 5 ESTs from 2-cell, 4-cell and 8-cell libraries, respectively. (**C**) Exon–intron structures and a putative protein structure of *Hmgpi*. *Hmgpi* has three exon–intron models and one protein model. Predicted protein domains are also shown. (**D**) Conserved domains of *Hmgpi/Ubtfl1* gene in mouse, rat and human. Pairwise alignment scores of conserved domains between species were shown. (**E**) Phylogenetic tree of gene nucleotide acid sequences containing HMG domains determined by a sequence distance method and the neighbour-joining (NJ) algorithm (41) using Vector NTI software (Invitrogen, Carlsbad, CA, USA).

stage (Fig. 2A). Furthermore, significant expression of *Hmgpi* was detected in ES cells, although not in embryonic carcinoma (EC) cells nor in mesenchymal stem cells (Fig. 2B). The relative abundance of *Hmgpi* transcripts in preimplantation embryos was measured by real-time quantitative RT–PCR (qRT–PCR) analysis (Fig. 2C). Four independent experiments were conducted with four replicates of 10 embryos each. To normalize the qRT–PCR reaction efficiency, *H2afz* was used as an internal standard (20). *Hmgpi* mRNA levels increased during the 1- to 2-cell stage, peaked at the 4-cell stage, and then gradually decreased during the 8-cell to blastocyst stage (Fig. 2C). The *in silico*-predicted preimplantation-stage-specific expression pattern of *Hmgpi* was therefore validated.

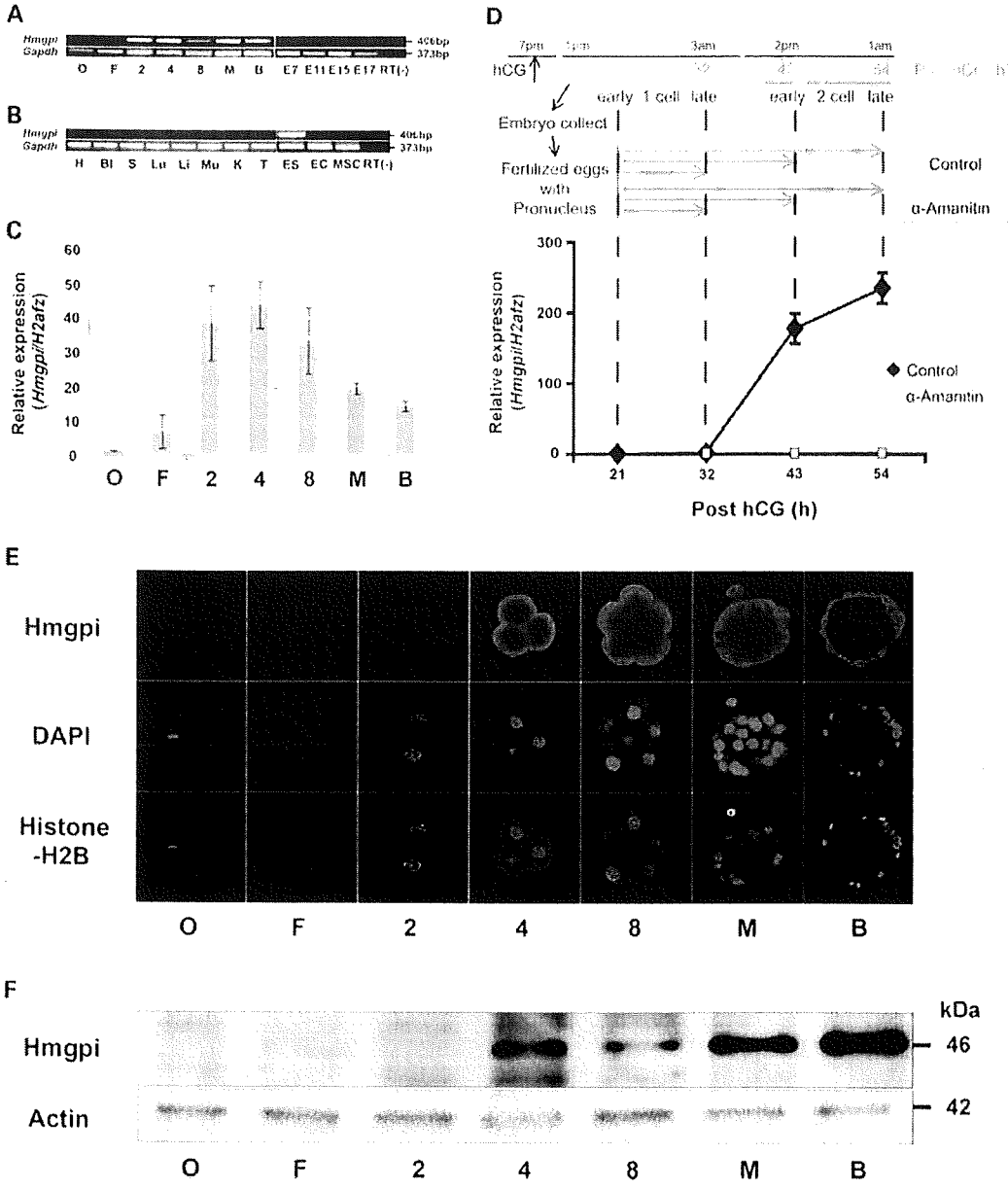


**Figure 2.** Expression of *Hmgpi* in preimplantation embryos and other tissues. (**A**) RT–PCR analysis of *Hmgpi* expression during preimplantation and postimplantation development (E7–E17). Three sets of 10 pooled embryos were collected from each stage (O: oocyte, F: fertilized egg, 2: 2-cell embryo, 4: 4-cell embryo, 8: 8-cell embryo, M: morula, and B: blastocyst) and used for RT–PCR analysis. The predicted sizes of the PCR products of *Hmgpi* and *Gapdh* are 406 and 373 bp, respectively. No PCR products were detected in the no-RT negative control (4-cell embryo). (**B**) RT–PCR analysis of *Hmgpi* expression in adult tissues, ES cells, EC cells and mesenchymal stem cells. mRNA was isolated from mouse tissues (H: heart, Bl: bladder, S: spleen, Lu: lung, Li: liver, Mu: muscle, K: kidney, T: testis, ES: ES cells, EC: EC cells, and MSC: mesenchymal stem cells). No PCR products were detected in the no-RT negative control (ES cells). (**C**) Real-time quantitative RT–PCR analysis of *Hmgpi* expression during preimplantation development. Fold differences in amounts of *Hmgpi* mRNA from the same numbers of oocytes (O), fertilized eggs (F), 2-cell embryos (2), 4-cell embryos (4), 8-cell embryos (8), morulae (M) and blastocysts (B) are shown after normalization to an internal reference gene (mouse *H2afz*). Values are means ± SE from four separate experiments. (**D**) *De novo* (zygotic) transcription of the *Hmgpi* gene. α-Amanitin studies revealed that *Hmgpi* is transcribed zygotically, but not maternally. *Hmgpi* expression was not observed before the 2-cell stage and α-amanitin completely inhibited *de novo* transcription at the 2-cell stage (closed rhombus: control group, open square: α-amanitin-treated group). The expression levels were normalized using *H2afz* as a reference gene. Values are means ± SE from four separate experiments. (**E**) Immunocytochemical analysis of HMGPI expression. MII oocytes and preimplantation embryos were immunostained with an anti-HMGPI antibody (red) and an anti-Histone-H2B antibody as a positive control of nuclear staining (green). Nuclei are shown by DAPI staining (blue). HMGPI protein was detected from 4-cell embryos to blastocysts. (**F**) Immunoblot analysis of HMGPI during preimplantation development. An amount of extracted protein corresponding to 100 oocytes or embryos was loaded per lane. Actin was used as a loading control. The representative result is shown from three independent experiments.

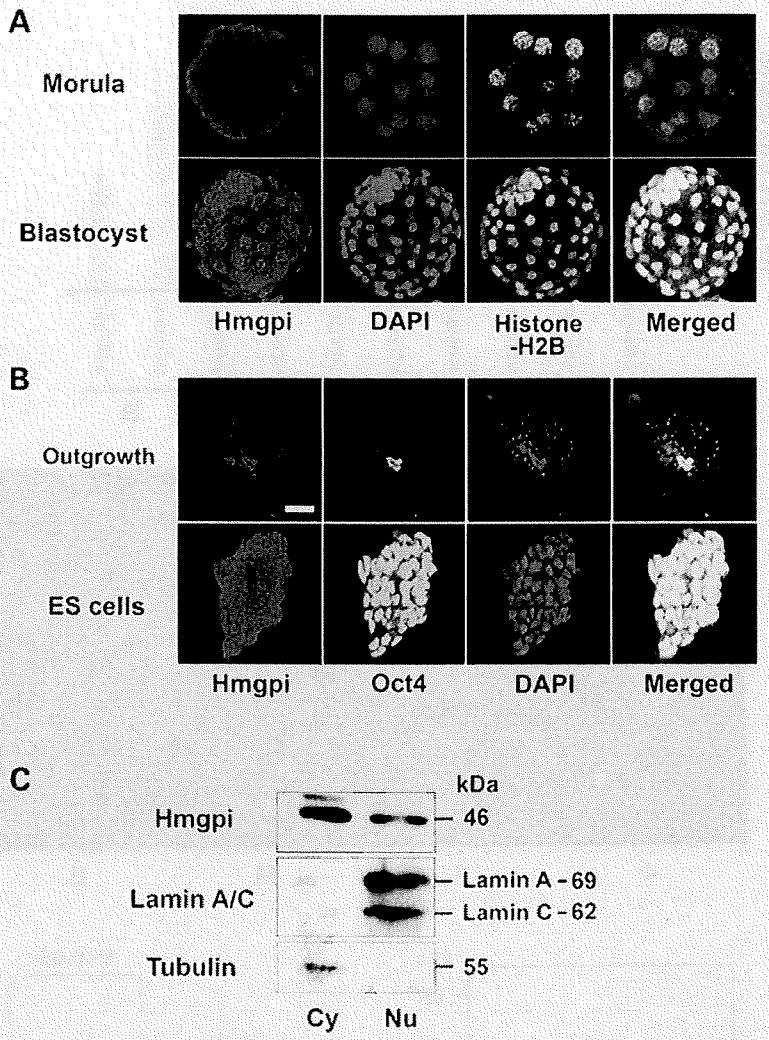


**Figure 3.** Localization of HMGPI in preimplantation embryos. (**A**) Nuclear translocation of HMGPI protein at the blastocyst stage. HMGPI was mainly detected in the cytoplasm of preimplantation embryos (from 4-cell embryos to morulae), but in the nuclei of blastocysts. Nuclei are shown by immunostaining with an anti-Histone-H2B antibody (green) and DAPI staining (blue). (**B**) Confocal microscopy images of blastocyst outgrowth and ES cells stained with antibodies to *Hmgpi* and *Oct4*, and with DAPI. Scale bar = 50 μM. (**C**) Western blotting analysis of HMGPI in cytoplasmic (Cy) and nuclear (Nu) fractions of ES cells. Lamin A/C and tubulin were used as markers of the nuclear and cytoplasmic fractions, respectively.

We then performed qRT–PCR analysis using α-amanitin to investigate *de novo* (zygotic) transcription of the *Hmgpi* gene. The supplementation of α-amanitin during *in vitro* culture from the 1-cell stage significantly reduced *Hmgpi* mRNA expression in the 2-cell embryos at post-hCG 43 and 53 h (early and late 2-cell stage, respectively) (Fig. 2D), implying that *Hmgpi* is transcribed zygotically during the major burst of ZGA, but not maternally.

To study the temporal and spatial expression pattern of the *Hmgpi*-encoded protein (HMGPI), we raised a polyclonal antibody against *Hmgpi* peptides. Western blot analysis of extracts from the mouse blastocysts showed only a single band corresponding to 46 kDa detected by the anti-HMGPI antibody. In addition, preincubation with the HMGPI peptide antigen abolished detection of the HMGPI protein, while preincubation with a control peptide had no effect on the immunodetection (Supplementary Material, Fig. S1). Although *Hmgpi* transcription started at the 2-cell stage, peaked at the 4-cell stage and then gradually decreased until the blastocyst stage (Fig. 2C), immunostaining and immunoblotting analysis revealed HMGPI expression from the 4-cell stage until the blastocyst stage, indicating a delayed expression pattern of HMGPI compared with that of the *Hmgpi* transcript. It was also notable that both ICM cells and trophectodermal cells retained HMGPI expression in blastocysts.

On the other hand, immunostaining for HMGPI in preimplantation embryos showed a unique subcellular localization pattern. Although a putative nuclear protein due to its role

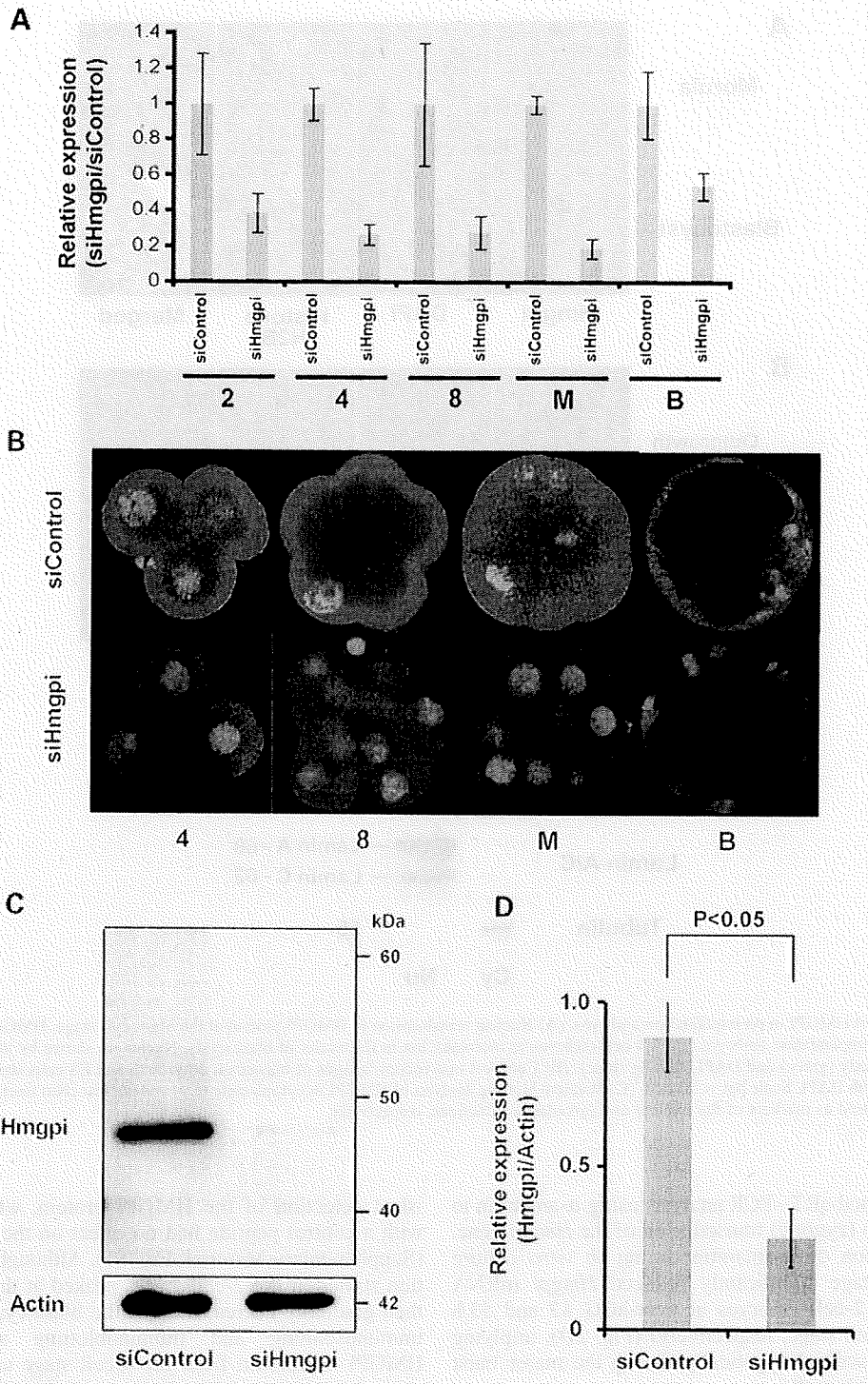


**Figure 4.** Loss-of-function study by siRNA technology. (**A**) Transcript levels of *Hmgpi* in embryos injected with control siRNA (siControl) and *Hmgpi* siRNA (siHmgpi) by real-time quantitative RT–PCR analysis. The expression levels were normalized using *H2afz* as a reference gene. Values are means ± SE for four separate experiments. (**B**) Laser scanning confocal microscopy images of HMGPI protein expression in a 4-cell embryo, 8-cell embryo, morula and blastocyst after injection with siControl or siHmgpi (red, HMGPI; blue, chromatin). (**C** and **D**) Immunoblot analysis of HMGPI expression at the blastocyst stage in siControl-injected and siHmgpi-injected embryos. The relative amount of HMGPI (46 kDa) was determined at the blastocyst stage (left: siControl-injected embryos, right: siHmgpi-injected embryos). The expression levels were normalized using actin expression (42 kDa) as a reference. Values are means ± SE from three separate experiments.

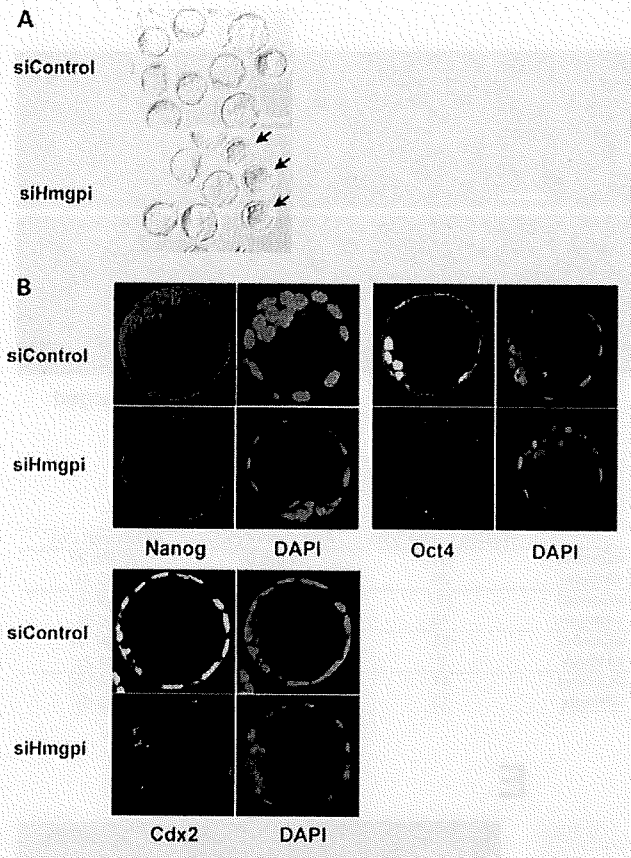


**Figure 5.** Function of *Hmgpi* in preimplantation development. (**A**) A pair of representative photos showing the development of embryos injected with *Hmgpi* siRNA (siHmgpi) and Control siRNA (siControl). The siHmgpi-injected embryos arrested at the morula stage are indicated by arrows. Scale bar = 100 μM. (**B**) For Nanog, Oct4 and Cdx2 immunostaining, all blastocysts in the siHmgpi-injected and siControl-injected groups were processed simultaneously. The laser power was adjusted so that the signal intensity was below saturation for the developmental stage that displayed the highest intensity and all subsequent images were scanned at that laser power. This allowed us to compare signal intensities for Nanog, Oct4 and Cdx2 expression between the siHmgpi-injected and siControl-injected embryos (Supplementary Material, Table S2).

as a transcription factor, HMGPI was detected mainly in the cytoplasm without any evidence of a nuclear localization from the 4-cell to the morula stage, suggesting a role other than transcriptional regulation (Fig. 2E). In contrast, HMGPI was localized to the nuclei rather than to the cytoplasm of blastocysts (Figs 2E and 3A). During blastocyst outgrowth, HMGPI was expressed in the nuclear region of most outgrowing cells, with scant amounts detected in the cytoplasm (Fig. 3B). Interestingly, Oct4-positive cells derived from the ICM showed particularly strong positive staining for HMGPI in the nucleus, suggesting a specific role as a nuclear protein in ES cells (Fig. 3B). On more closely examining HMGPI in ES cells, we found that almost all the Oct4-positive undifferentiated ES cells in a colony also expressed HMGPI (Fig. 3B), and immunoblotting confirmed HMGPI expression in both nuclear and cytoplasmic fractions of ES cells (Fig. 3C).

### Effect of siRNA on *Hmgpi* mRNA level and protein synthesis

To investigate a role of *Hmgpi* in early embryonic development, we knocked down *Hmgpi* expression in mouse preimplantation embryos. We employed an oligonucleotide-based siRNA (denoted here siHmgpi and obtained from PE Applied Biosystems, Foster City, CA, USA). Zygotes injected with *Hmgpi* siRNAs (siHmgpi) or control siRNA (siControl) and non-injected zygotes as negative controls were cultured. *Hmgpi* expression was severely suppressed in the siHmgpi-injected embryos, and significantly lower than those in the siControl-injected or non-injected embryos (Fig. 4A). The siControl-injected embryos did not show any difference from the non-injected embryos in *Hmgpi* expression (data not shown). In addition, immunofluorescent staining clearly demonstrated that the siRNA injection reduced HMGPI protein expression in an individual preimplantation embryo (Fig. 4B). In the same set of experiments, the HMGPI levels were also assayed by western blotting (Figs 4C and 4D). HMGPI expression was significantly reduced in siHmgpi-injected blastocysts ($0.89 \pm 0.10$) compared with that in negative controls ($0.28 \pm 0.08$; $P < 0.05$).

Furthermore, we confirmed that siHmgpi had no influence on the expression of other genes with sequence similarities to *Hmgpi*, namely *Ubtf*, *Hmgb1*, *Hmgb2* and *Hmgb3*. Although *Ubtf*, *Hmgb1*, *Hmgb2* and *Hmgb3* were all expressed in control preimplantation embryos, the siHmgpi construct used in this study did not affect the expression of these genes in the siHmgpi-injected embryos (Supplementary Material, Fig. S2). On the other hand, it has been demonstrated that loss-of-function of these genes produces no distinct phenotypes at the pre- and peri-implantation stages (21).

### Effect of *Hmgpi* siRNA on preimplantation development

To study the function of *Hmgpi* during preimplantation development, siHmgpi-injected or siControl-injected zygotes were cultured *in vitro* until the blastocyst stage. The embryos injected with siHmgpi at 21–23 h after hCG administration often failed to become blastocysts at 3.5 days postcoitum (dpc) (Fig. 5A). In addition, the reduction in Hmgpi expression significantly suppressed preimplantation development, whereby $68.9 \pm 1.3\%$ of siHmgpi-injected embryos became blastocysts, while $94.1 \pm 1.3\%$ of siControl-injected embryos reached the blastocyst stage (Supplementary Material, Fig. S3; $P < 0.0001$). Most of the siHmgpi-injected embryos that failed to become blastocysts showed developmental arrest after the morula stage and did not appear to form blastocoels, suggesting impairment of trophectodermal development (Supplementary Material, Fig. S3). To analyze the phenotype of siHmgpi-injected embryos further, we performed immunofluorescence staining of lineage-specific markers such as Cdx2, Nanog and Oct4 at the blastocyst stage. Although siHmgpi-injected embryos that reached the blastocyst stage appeared morphologically intact, the expression of lineage-specific markers was reduced (Fig. 5B). Cdx2, which is required for implantation and extra-embryonic development, was particularly and markedly down-regulated in trophectodermal cells, while Nanog and Oct4

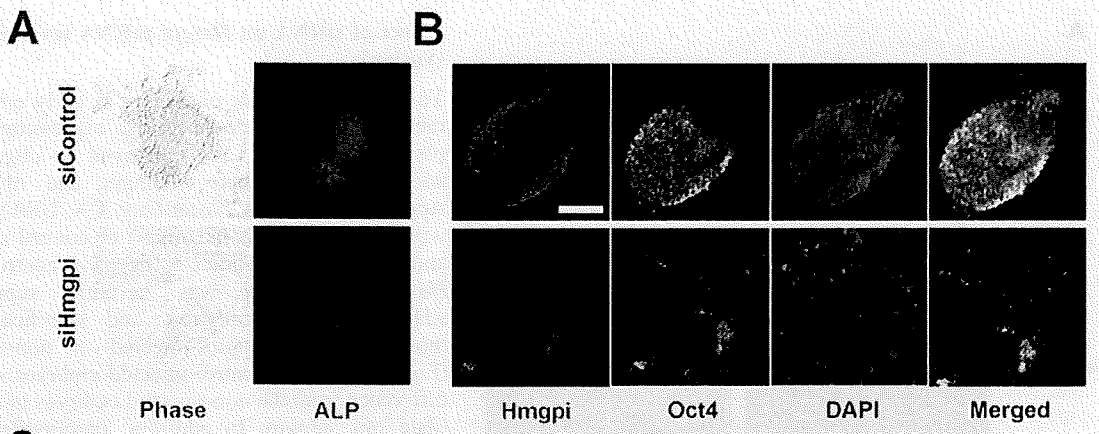


C

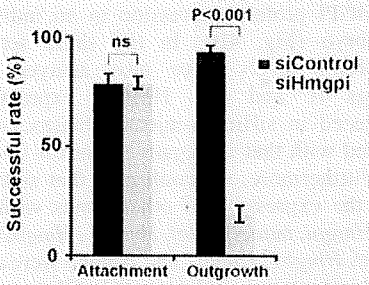


| | Tested blastocysts | Attachment (%) | Outgrowth (%) |
|---|---|---|---|
| siControl | 51 | 34 (66.6) | 30 (88.2) |
| siHmgpi | 20 | 15 (75.0) | 2 (13.3) |
| siControl | 117 | 92 (78.6) | 80 (86.9) |
| siHmgpi | 13 | 10 (76.9) | 2 (20.0) |
| siControl | 55 | 49 (89.0) | 48 (97.9) |
| siHmgpi | 8 | 7 (87.5) | 1 (14.2) |
| siControl | 41 | 33 (80.4) | 33 (100.0) |
| siHmgpi | 13 | 10 (76.9) | 3 (30.0) |

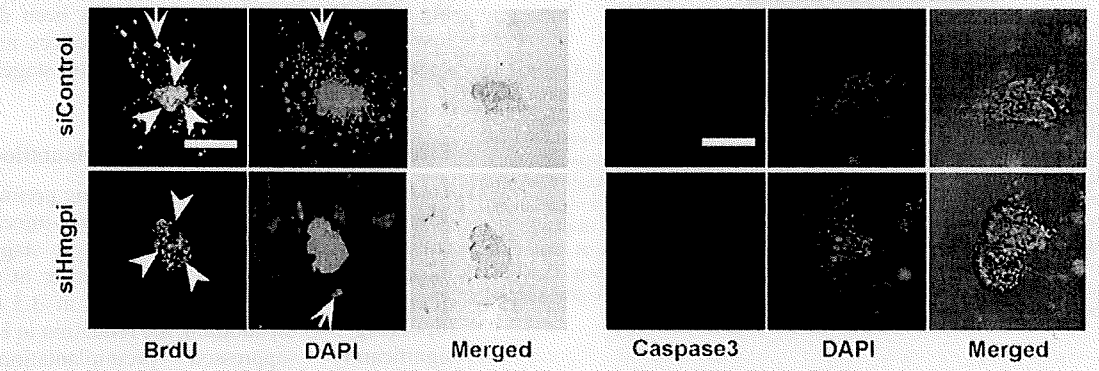


F

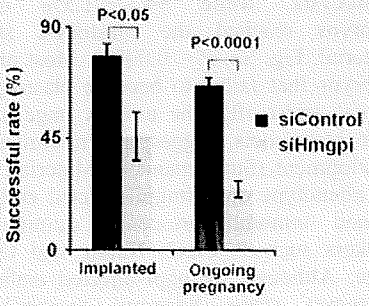


| | Transferred embryos | Implanted (%) | Ongoing pregnancy (%) |
|---|---|---|---|
| siControl | 30 | 23 (76.7) | 20 (66.7) |
| siHmgpi | 18 | 6 (33.3) | 3 (16.7) |
| siControl | 30 | 25 (83.3) | 18 (60.0) |
| siHmgpi | 32 | 20 (62.5) | 10 (31.2) |
| siControl | 16 | 13 (81.2) | 12 (75.0) |
| siHmgpi | 24 | 15 (62.5) | 7 (29.1) |
| siControl | 20 | 13 (65.0) | 13 (65.0) |
| siHmgpi | 32 | 8 (25.0) | 7 (21.8) |

were likewise downregulated in ICM cells of the siHmgpi-injected embryos (Fig. 5B and Supplementary Material, Table S2). Thus, *Hmgpi* is essential for the earliest embryonic development; both ICM and trophectodermal development.

### Effect of *Hmgpi* siRNA on *in vivo* and *in vitro* peri-implantation development

To investigate the role of *Hmgpi* in proliferation of the ICM and trophectodermal cells, siHmgpi-injected and siControl-injected embryos were further cultured *in vitro* from the blastocyst stage, and attachment and outgrowth of each embryo on gelatin-coated culture plates was examined. HMGPI expression in siHmgpi-injected embryos was significantly reduced, and immunostaining showed that many colonies of ICM cells in the embryos collapsed during outgrowth culture (Fig. 6A and B). Although the vast majority of ICMs from siControl-injected embryos showed successful attachment (80.3 $\pm$ 4.9%) and vigorous outgrowth (96.2 $\pm$ 2.7%), those from siHmgpi-injected embryos failed to proliferate or produced only a residual mass (19.3 $\pm$ 3.8%) despite successfully attaching (79.0 $\pm$ 2.8%) (Fig. 6C; attachment ns; outgrowth, $P < 0.001$). These results implied that *Hmgpi* is essential for proliferation of ICM and trophectodermal cells in peri-implantation development, and for derivation of ES cells.

We then investigated cell proliferation and apoptosis during blastocyst outgrowth. Comparable incorporation of BrdU in blastocyst outgrowths of siHmgpi-injected embryos was less than that of siControl-injected embryos. Proliferation was significantly reduced in ICM-derived cells and dramatically suppressed in trophoblast cells (Fig. 6D). Embryonic fibroblasts were used as a feeder layer in this study and could support ICM cells, thus proliferation should have proceeded regardless of trophectodermal cell support. Therefore, the collapsed ICM-derived colonies in the current experiment were not a secondary effect of reduced proliferation in trophoblast cells, but a direct effect of the siHmgpi-induced decrease in ICM proliferation. Apoptosis was not detected in any cells during blastocyst outgrowth of siHmgpi-injected embryos, based on the absence of active caspase3 (Fig. 6E). Taken together, these findings show that *Hmgpi* is indispensable for proliferation of the ICM and trophectodermal cells in peri-implantation development and for the generation of ES cells.

Finally, we tested whether the experimental blastocysts could develop *in vivo* by transferring siHmgpi-injected and siControl-injected blastocysts into the uterus of pseudopregnant mice. Only 45.8 $\pm$ 9.7 and 24.7 $\pm$ 3.3% of blastocysts injected with siHmgpi implanted and developed, respectively, whereas most of the siControl-injected embryos showed successful implantation and ongoing development (76.5 $\pm$ 4.0 and 66.6 $\pm$ 3.3%, respectively) (Fig. 6F; implanted, $P < 0.05$; ongoing pregnancy, $P < 0.0001$). These results confirmed a role for *Hmgpi* in peri-implantation embryonic development.

## DISCUSSION

We previously analyzed the dynamics of global gene expression changes during mouse preimplantation development (3). Understanding these preimplantation stages is important for both reproductive and stem cell biology. Many genes showing wave-like activation patterns (e.g. ZGA and MGA) during preimplantation were identified, and any or all of these may contribute to the complex gene regulatory networks. *Hmgpi*, one of the few novel preimplantation-specific genes, is involved in early development, implantation and ES cell derivation.

### Structure-based prediction of *Hmgpi* function

Structural information about a protein sometimes hints at functional mechanisms, which remain unknown for *Hmgpi*'s clear role in early embryonic development. The HMG family proteins are abundant nuclear proteins that bind to DNA in a non-sequence-specific manner, influence chromatin structure and enhance the accessibility of binding sites to regulatory factors (17). Based on the number and the type of HMG domains, *Hmgpi* is relevant to the HMGB subfamily, characterized by containing two HMG-box domains ('HMG-box' or 'HMG-UBF_HMG-box'), rather than either the HMGA or HMGN subgroups. *Hmgpi* is also known as *Ubtfl1* in the NCBI gene database, based on sequence similarity to *Ubtf*, a well-known ZGA gene (3,22). *Ubtf*, encoding a SANT domain and six HMG-box domains, functions exclusively in RNA polymerase I (Pol I) transcription (23) and acts through its multiple HMG boxes to induce looping of DNA, which creates a nucleosome-like structure to modulate tran-

**Figure 6.** Function of *Hmgpi* in peri-implantation development. (**A**) Blastocyst outgrowth and alkaline phosphatase (AP) activity in the siHmgpi-injected and siControl-injected embryos, carried out according to a standard procedure (42). Representative images of phase-contrast microscopy for blastocyst outgrowth and fluorescent immunocytochemistry for AP are shown. Scale bar = 100 μM. (**B**) Confocal microscopy images of blastocyst outgrowth for the siHmgpi-injected and siControl-injected embryos, stained with antibodies to Hmgpi and Oct4. Nuclei are shown by DAPI staining. Scale bar = 100 μM. (**C**) Successful rate of blastocyst outgrowth for siHmgpi-injected and siControl-injected embryos. Successful outgrowth in this assay was indicated by the presence of proliferating cells after 6 days in culture. The experiment was repeated four times. (**D**) BrdU incorporation assay for blastocyst outgrowth of the siHmgpi-injected and siControl-injected embryos. Cell proliferation was determined by BrdU incorporation (ICM: arrowhead, trophectodermal cells: arrow). The trophectodermal component contained few cells and BrdU incorporation was confined to the ICM core; however, cell proliferation was reduced in the blastocyst outgrowth of siHmgpi-injected embryos compared with that of the siControl-injected embryos. Nuclei are shown by DAPI staining. Scale bar = 100 μM. (**E**) Immunocytochemistry with an anti-caspase3 antibody in blastocyst outgrowth of the siHmgpi-injected and siControl-injected embryos. Apoptotic cells were not apparent in the blastocyst outgrowth of either injected embryo. Nuclei are shown by DAPI staining. Scale bar = 100 μM. (**F**) Successful rate of siHmgpi-injected and siControl-injected embryo transfer. We transferred 3.5 dpc blastocysts into the uteri of 2.5 dpc pseudopregnant ICR female mice. The pregnant ICR mice were sacrificed on day 12.5 of gestation and the total numbers of implantation sites and of live and dead embryos/fetuses were counted. The experiment was repeated four times.

scription of the 45S precursor of ribosomal RNA (rRNA) by Pol I (24,25). Because the association of UBTF with rRNA genes *in vivo* is not restricted to the promoter and extends across the entire transcribed portion, UBTF promotes the formation of nucleolar organizer regions, indicative of 'open' chromatin (26). Based on the sequence similarity between UBTF and HMGPI, HMGPI might also bind to DNA in a non-specific manner, and modulate chromatin during peri-implantation when dynamic chromatin change is essential.

Alternatively, HMGPI may act as a cytokine during preimplantation development in a similar manner to HMGB1. HMGB proteins are found primarily in the cell nucleus, but also to varying extents in the cytosol (27,28), and have been suggested to shuttle between compartments (17). HMGB1 is indeed passively released from nuclei upon cell death and actively secreted as a cytokine (29), and the addition of recombinant HMGB1 into culture medium enhances *in vitro* development of mouse zygotes to the blastocyst stage in the absence of BSA supplementation (30). Although HMGPI failed to be detected in culture media after *in vitro* culture of preimplantation embryos or ES cells in this study (data not shown), two different modes of Hmgpi action, chromatin modulator and secreted mediator, should be taken into consideration as discussed later.

### Role of *Hmgpi* during peri-implantation

The HMGPI protein was first detected in 4-cell embryos and then abundantly expressed in 8-cell embryos, morulae, ICM, trophectoderm and ES cells. Although *Hmgpi* transcription peaked at the 4-cell stage, the most dramatic siRNA effect appeared at the blastocyst and subsequent stages. This discrepancy between temporal expression and phenotype is attributed to three possible mechanisms. First, protein expression is generally delayed from transcription, indicated here by the *Hmgpi* transcripts and HMGPI protein expression peaking at the 4-cell stage and blastocyst stage, respectively. Similarly, *Stella* (31) and *Pms2* (32) are maternal-effect genes, but do not cause developmental loss until later preimplantation stages. A second possibility is the incompleteness of siRNA knockdown. One limitation of such knockdown experiments is the potential variability in levels of silencing of a target gene, which could in turn underlie the observed phenotypic variability in the present study. Embryos with complete suppression of Hmgpi may exhibit developmental arrest at earlier stages (e.g. at the morula stage), while those with less suppression may not display a phenotype until the later stages (e.g. at the implantation stage). Ideally, the suppression level of each embryo could be experimentally analyzed to correlate with the phenotype. The third possibility is spatial translocation of HMGPI protein in the blastocyst cells. The HMGPI expression pattern indicated differential spatial requirements during early embryogenesis, supported by the apparent ability of HMGPI to shuttle between the nucleus and the cytoplasm; the cytoplasmic HMGPI observed from the 4-cell to morula stages and the nuclear HMGPI in blastocysts and ES cells could have different functions. A bipartite nuclear localization signal (NLS) peptide (FKKEKEDFQKKMRQFKK) similar to NLS of HMGN2/HMG-17 (33) is also present in the HMGPI sequence. Thus, the nuclear HMGPI in blastocysts and ES cells might exert a critical transcriptional role to regulate gene expression essential for peri-implantation development. Indeed, the siHmgpi-induced knockdown of *Hmgpi* expression downregulated *Cdx2* in trophectodermal cells and *Oct4* and *Nanog* in ICM cells, with subsequently reduced proliferation of trophectodermal cells and ICM-derived cells during blastocyst outgrowth.

### Genes indispensable for derivation of ES cells

Like *Hmgpi*, *Zscan4* is another exclusively zygotic gene not expressed at any other developmental stage (13). *Zscan4* is a putative transcription factor harboring a SCAN domain and zinc finger domains, and transcribed not only in preimplantation embryos but also in ES cells (13). Reduction of *Zscan4* by RNA interference showed a phenotype similar to that induced by *Hmgpi* knockdown: developmental deterioration at the preimplantation stages, especially cleavage pause at 2-cell stage, and failure in blastocyst outgrowth, ES-cell derivation and implantation. Thus, a preimplantation-specific gene expression pattern could indicate a function in ES-cell derivation and/or maintenance. Indeed, *Hmgpi* was also expressed in entire ES colonies, whereas *Zscan4* shows a peculiar mosaic expression pattern in undifferentiated ES cell colonies. Furthermore, the *Hmgpi* gene is highly expressed in ES cells, but not in EC cells; *Hmgpi* is thus eligible as a putative ECAT (ES cell-associated transcript), whose ESTs are overrepresented in cDNA libraries from ES cells compared with those from somatic tissues and other cell lines including EC cells (34). It is also likely that *Hmgpi* is expressed in iPS cells, based on *in silico* analyses of expression profiles [NCBI GEO database, e.g. GSE10806 (35)]. Thus, *Hmgpi* is likely to have a role in maintaining pluripotent cells, since the ECATs such as *Nanog*, *Eras* and *Gdf3* are required for pluripotency and proliferation of ES cells (34,36,37). In the current study, *Hmgpi* was indeed involved in blastocyst outgrowth of ICM cells. On the other hand, several genes including ECAT members have been implicated in trophectodermal development as well as in early embryonic development. Like *Hmgpi* that was expressed in both ICM cells and trophectodermal cells, *Dnmt3l/Ecat7* has a role in embryonic and extra-embryonic tissues in early developmental stages. *DNMT3L* is recruited by *DNMT3A2* to chromatin (38) to function in DNA methylation in ES cells, and defects in maternal *DNMT3L* induce a differentiation defect in the extra-embryonic tissue (39). The reduced CDX2 expression in blastocysts and poor BrdU incorporation during blastocyst outgrowth following siHmgpi knockdown suggested the potential involvement of *Hmgpi* in trophectodermal development.

In summary, *Hmgpi* is required early on in mammalian development to generate healthy blastocysts that implant successfully and produce ES cells. HMGPI translocates into the nucleus from cytoplasm at the blastocyst stage, which is importantly a turning point of early embryonic development when DNA-methylation levels are at their lowest and implantation takes place. The nuclear HMGPI in blastocysts and ES cells is expected to act as a transcription factor to regulate gene expression networks underlying the generation, self-renewal and maintenance of pluripotent cells. Because E7 embryos have already stopped expressing *Hmgpi*, it is likely

that *Hmgpi* stage-specifically regulates a set of genes that drive peri-implantation development. It will be valuable to identify both cofactors that bind HMGPI and recognize specific DNA sequences, as well as genes that are regulated by *Hmgpi* using ES cells. A better understanding of the *Hmgpi* transcriptional network will also improve culture methods for healthy blastocysts and for generating, maintaining and differentiating ES cells.

## MATERIALS AND METHODS

### Identification of the mouse *Hmgpi* gene by *in silico* analysis

Preimplantation-specific genes were identified based on global gene expression profiling of oocytes and preimplantation embryos (3,40) and expressed sequence tag (EST) frequencies in the Unigene database. SMART (19) was used for domain prediction analysis. Orthologous relationships between HMG family genes were identified from phylogenetic-tree amino acid sequences determined by a sequence distance method and the Neighbor Joining (NJ) algorithm (41) using Vector NTI software (Invitrogen, Carlsbad, CA, USA).

### Collection and manipulation of embryos

Six- to 8-week-old B6D2F1 mice were superovulated by injecting 5 IU of pregnant-mare serum gonadotropin (PMS; Calbiochem, La Jolla, CA, USA) followed by 5 IU of human chorionic gonadotropin (HCG; Calbiochem) 48 h later. The Institutional Review Board of the National Research Institute for Child Health and Development, Japan granted ethics approval for embryo collection from the mice. Unfertilized eggs were harvested 18 h after the HCG injection by a standard published method (42), and the cumulus cells were removed by incubation in M2 medium (EmbryoMax M-2 Powdered Mouse Embryo Culture Medium; Millipore, Billerica, MA, USA) supplemented with 300 μg/ml hyaluronidase (Sigma-Aldrich, St Louis, MO, USA). The eggs were then thoroughly washed, selected for good morphology and collected. Fertilized eggs were also harvested from mated superovulated mice in the same way as unfertilized eggs and embryos with two pronuclei (PN) were collected to synchronize *in vitro* embryo development. Fertilized eggs were cultured in synthetic oviductal medium enriched with potassium (EmbryoMax KSOM Powdered Mouse Embryo Culture Medium; Millipore) at 37°C in an atmosphere of 95% air/5% $CO_2$. Cultured blastocysts were transferred into pseudopregnant recipients as described previously (42). We transferred 3.5 dpc blastocysts into the uteri of 2.5 dpc pseudopregnant ICR female mice. RNA interference experiments were carried out by microinjecting $<10$ pl (25 ng/μl) of oligonucleotides (siHmgpi and siControl) into the cytoplasm of zygotes. The optimal siRNAs were determined by testing different concentrations (5, 10, 25 and 50 ng/μl) of three siRNAs (PE Applied Biosystems, Foster City, CA, USA), resuspended and diluted with the microinjection buffer (Millipore). Their target sequences are listed in Supplementary Material, Table S3. More than 10 independent experiments were performed to study the effect of *Hmgpi* knockdown on preimplantation development and implantation.

### Culture of ES cells and blastocyst outgrowth

A mouse ES cell line (B6/129ter/sv line) was first cultured for two passages on gelatin-coated culture dishes in the presence of leukemia inhibitory factor (LIF) to remove contaminating feeder cells. Cells were then seeded on gelatin-coated 6-well plates at a density of $1-2 \times 10^5$/well ($1-2 \times 10^4$/cm$^2$) and cultured for 3 days in complete ES medium: KnockOut DMEM (Invitrogen) containing 15% KnockOut Serum Replacement (KSR; Invitrogen), 2000 U/ml ESGRO (mLIF; Chemicon, Temecula, CA, USA), 0.1 mM non-essential amino acids, 2 mM GlutaMax (Invitrogen), 0.1 mM beta-mercaptoethanol (2-ME; Invitrogen) and penicillin/streptomycin (50 U/50 μg/ml; Invitrogen). Blastocyst outgrowth experiments were carried out according to a standard procedure (42). In brief, zona pellucidae of blastocysts at 3.5 dpc were removed using acidic Tyrode's solution (Sigma). The blastocysts were cultured individually in the ES medium on gelatinized chamber slides at 37°C in an atmosphere of 5% $CO_2$. The cultured cells were examined and photographed daily. Alkaline phosphatase activity was measured using a specific detection kit (Vector Laboratories, CA, USA) after 6 days in culture. Four independent experiments were performed.

### Immunostaining of oocytes and preimplantation embryos

Samples were fixed in 4% paraformaldehyde (Wako Pure Chemical, Osaka, Japan) with 0.1% glutaraldehyde (Wako) in phosphate-buffered saline (PBS) for 10 min at room temperature (RT), and then permeabilized with 0.5% Triton X-100 (Sigma) in PBS for 30 min. Immunocytochemical staining was performed by incubating the fixed samples with primary antibodies for 60 min, followed by secondary antibodies for 60 min. A polyclonal antibody to mouse HMGPI was raised in rabbits against three synthesized peptides designed according to sequence specificity, homology between mouse and human HMGPI, antigenicity, hydrophilicity and synthetic suitability [(i) CIQGHHDGAQSSRQDFTD, (ii) CMSMSGG RSSKFGRTEQS, (iii) ESPRTVSSDMKFQGC; Medical & Biological Laboratories Co, Nagoya, Japan). The anti-HMPGI was used at 1:300 dilution, followed by Alexa Fluor 546 goat anti-rabbit IgG (Molecular Probes, Invitrogen) as the secondary antibody. The anti-Histone H2B antibody (Medical & Biological Laboratories Co, Nagoya, Japan) was used at 1:300 dilution as positive control of nuclear staining, followed by Alexa Fluor 488 goat anti-mouse IgG (Molecular Probes, Invitrogen) as the secondary antibody. Blastocysts were immunostained using a monoclonal anti-Oct4 antibody (mouse IgG2b isotype, 200 μg/ml; Santa Cruz Biotechnology, Santa Cruz, CA, USA), rabbit polyclonal anti-Nanog antibody (ReproCELL, Tokyo, Japan), mouse monoclonal anti-Cdx2 antibody (CELL MARQUE, Rocklin, CA, USA), mouse monoclonal anti-BrdU antibody (Santa Cruz) and rabbit monoclonal anti-active caspase 3 (Abcam) antibody, all diluted at 1:50–300. The appropriate secondary antibodies (IgG) were diluted at 1:300 and supplied by Molecular Probes/Invitrogen: goat anti-rabbit IgG conjugated with Alexa Fluor 546 and goat anti-mouse IgG(H + L) conjugated with Alexa Fluor 488. The cellular DNA (nuclei) was stained with 4′,6-diamidino-2-phenylindole (DAPI; Wako; diluted

1:300). The cells were then washed with PBS and viewed by laser confocal microscopy (LSM510, Zeiss). For HMGPI immunostaining, all samples were processed simultaneously. The laser power was adjusted so that the signal intensity was below saturation for the developmental stage that displayed the highest intensity and all subsequent images were scanned at that laser power. This allowed us to compare signal intensities for HMGPI expression at different developmental stages. The other molecules in blastocysts and outgrowth were viewed and imaged as for the HMGPI expression.

### Immunocytochemistry of blastocyst outgrowths and ES cells

Cultured ES cells and blastocyst outgrowths were fixed with 4% paraformaldehyde for 10 min at 4°C, treated with 0.1% Triton X-100 (Sigma) in PBS for 15 min at RT, and then incubated for 30 min at RT in protein-blocking solution consisting of PBS supplemented with 5% normal goat serum (Dako, Glostrup, Denmark). The samples were then incubated overnight with the primary antibodies to OCT4, HMGPI, BrdU or active caspase 3 in PBS at 4°C. The cells were then extensively washed in PBS and incubated at RT with Alexa Fluor 488 goat anti-mouse IgG1 (anti-OCT4 and anti-BrdU antibodies, diluted 1:300; Molecular Probes) or Alexa Fluor 546 goat anti-rabbit IgG(H + L) (anti-HMGPI and anti-caspase 3 antibodies, diluted 1:300), and nuclei were counterstained with DAPI for 30 min. To prevent fading, cells were then mounted in Dako fluorescent mounting medium (Dako).

### Incorporation of bromodeoxyuridine (BrdU)

E3.5 blastocysts and blastocyst outgrowths were cultured for 16 h in KSOM and ES medium, respectively, supplemented with 10 μM BrdU (Sigma). Samples were then fixed in 4% paraformaldehyde for 20 min, washed in PBS and then treated with 0.5 M HCl for 30 min.

### RNA extraction and real-time quantitative reverse transcriptase (qRT)–PCR

Embryos for qRT–PCR analysis were collected at 18 h post-hCG and cultured as described above. They were harvested at 0.5, 1.25, 1.75, 2.25, 2.75 and 3.75 dpc to obtain fertilized eggs 2-cell, 4-cell, 8-cell, morula and blastocyst embryos, respectively. Three subsets of 10 and 50 synchronized and intact embryos were transferred in PBS supplemented with 3 mg/ml polyvinylpyrrolidone (PVP) and stored in liquid nitrogen. Total RNA from 10 and 50 embryos was extracted using the PicoPure RNA Isolation Kit (Arcturus, La Jolla, CA, USA). The reverse transcription reaction, primed with polyA primer, was performed using Superscript III reverse transcriptase (Invitrogen) following the manufacturer's instructions. Total RNA isolated was reverse transcribed in a 20 μl volume. The resulting cDNA was quantified by qRT–PCR analysis using the SYBR Green Realtime PCR Master Mix (Toyobo, Osaka, Japan) and ABI Prism 7700 Sequence Detection System (PE Applied Biosystems) as described previously (43). An amount of cDNA equivalent to 1/2 an embryo was used for each real-time PCR reaction with a minimum of three replicates, with no-RT and no-template controls for each gene. Data were normalized against *H2afz* by the ΔΔCt method (44). PCR primers for the genes of *Hmgpi, H2afz* and *Gapdh* were listed in Supplementary Material, Table S4. Calculations were automatically performed by ABI software (Applied BioSystems). For alpha-amanitin studies, fertilized eggs were first harvested at 18 h post-hCG, instead of eggs already advanced to the two-pronucleus stage. After 3 h of incubation, eggs that carried both male and female pronuclei were selected at 21 h post-hCG and randomly assigned to two experimental groups: with and without addition of alpha-amanitin to the culture medium. The eggs were further cultured in KSOM at 37°C in an atmosphere of 5% $CO_2$ until the specified time point (32, 43 and 54 h post-hCG). Embryos used for alpha-amanitin studies and RNA interference experiments were subjected to qRT–PCR as described for the normal preimplantation embryos.

### Immunoblot analysis

Protein samples from embryos were solubilized in Sample Buffer Solution without 2-ME (Nacalai Tesque, Kyoto, Japan), resolved by NuPAGE Novex on Tris-acetate mini gels (Invitrogen), and transferred to Immobilon-P transfer membrane (Millipore). The membrane was soaked in protein blocking solution (Blocking One solution, Nacalai) for 30 min at RT before an overnight incubation at 4°C with primary antibody, also diluted in blocking solution. The membrane was then washed three times with TBST (Tris-buffered saline with 0.1% Tween-20), incubated with a horseradish peroxidase-conjugated secondary antibody (0.04 μg/ml) directed against the primary antibody for 60 min, and washed three times with TBST. The signal was detected by enhanced chemiluminescence (SuperSignal West Dura Extended Duration Substrate, Thermoscientific, Rockford, IL, USA) following the manufacturer's recommendations. The intensity of the band was quantified using NIH Image J software. Briefly, the signal was outlined and the mean intensity and background fluorescence were measured. The specific signal was calculated by dividing the band intensities for HMGPI by those for actin.

### Statistical analysis

Differences between groups were evaluated statistically using Student's *t*-test or ANOVA, with *P*-values $< 0.05$ considered significant.

## SUPPLEMENTARY MATERIAL

Supplementary Material is available at *HMG* online.

## ACKNOWLEDGEMENTS

The authors would like to thank Dr Takashi Hiiragi for valuable advice and critical reading of the manuscript.

*Conflict of Interest statement*. The authors declare that there is no conflict of interest that would prejudice the impartiality of the scientific work.

## FUNDING

This work was supported, in part, by Grants-in-Aid from the Japan Society for the Promotion of Science (19591911 to T.H., 21390456 to H.A.), by a National Grant-in-Aid from Japanese Ministry of Health, Labor, and Welfare (H21-001, H20-001 to T.H., H18-004 to H.A. and N.K.) and by a Grant-in-Aid from the Yamaguchi- Endocrine Organization to T.H. Funding to pay the Open Access publication charges for this article was provided by Grants-in-Aid for Young Scientists (B) (21791581 to M.Y.).

## REFERENCES

1. DePamphilis, M.L., Kaneko, K.J. and Vassilev, A. (2002) Activation of zygotic gene expression in mammals. DePamphilis, M.L. (ed.), *Advances in Developmental Biology and Biochemistry*, Vol. 12, Elsevier Science, B.V.
2. Latham, K.E. and Schultz, R.M. (2001) Embryonic genome activation. *Front. Biosci.*, **6**, D748–D759.
3. Hamatani, T., Carter, M.G., Sharov, A.A. and Ko, M.S. (2004) Dynamics of global gene expression changes during mouse preimplantation development. *Dev. Cell.*, **6**, 117–131.
4. Takahashi, K. and Yamanaka, S. (2006) Induction of pluripotent stem cells from mouse embryonic and adult fibroblast cultures by defined factors. *Cell*, **126**, 663–676.
5. Hamatani, T., Yamada, M., Akutsu, H., Kuji, N., Mochimaru, Y., Takano, M., Toyoda, M., Miyado, K., Umezawa, A. and Yoshimura, Y. (2008) What can we learn from gene expression profiling of mouse oocytes? *Reproduction*, **135**, 581–592.
6. Ko, M.S., Kitchen, J.R., Wang, X., Threat, T.A., Hasegawa, A., Sun, T., Grahovac, M.J., Kargul, G.J., Lim, M.K., Cui, Y. *et al.* (2000) Large-scale cDNA analysis reveals phased gene expression patterns during preimplantation mouse development. *Development*, **127**, 1737–1749.
7. Okazaki, Y., Furuno, M., Kasukawa, T., Adachi, J., Bono, H., Kondo, S., Nikaido, I., Osato, N., Saito, R., Suzuki, H. *et al.* (2002) Analysis of the mouse transcriptome based on functional annotation of 60,770 full-length cDNAs. *Nature*, **420**, 563–573.
8. Solter, D., de Vries, W.N., Evsikov, A.V., Peaston, A.E., Chen, F.H. and Knowles, B.B. (2002) Fertilization and activation of the embryonic genome. Rossant, J. and Tam, P.P.L. (eds), *Mouse Development: Patterning, Morphogenesis, and Organogenesis.*, Academic Press, San Diego, pp. 5–19.
9. Wang, Q.T., Piotrowska, K., Ciemerych, M.A., Milenkovic, L., Scott, M.P., Davis, R.W. and Zernicka-Goetz, M. (2004) A genome-wide study of gene activity reveals developmental signaling pathways in the preimplantation mouse embryo. *Dev. Cell.*, **6**, 133–144.
10. Wang, S., Cowan, C.A., Chipperfield, H. and Powers, R.D. (2005) Gene expression in the preimplantation embryo: in-vitro developmental changes. *Reprod. Biomed. Online*, **10**, 607–616.
11. Zeng, F., Baldwin, D.A. and Schultz, R.M. (2004) Transcript profiling during preimplantation mouse development. *Dev. Biol.*, **272**, 483–496.
12. Choo, K.B., Chen, H.H., Cheng, W.T., Chang, H.S. and Wang, M. (2001) In silico mining of EST databases for novel pre-implantation embryo-specific zinc finger protein genes. *Mol. Reprod. Dev.*, **59**, 249–255.
13. Falco, G., Lee, S.L., Stanghellini, I., Bassey, U.C., Hamatani, T. and Ko, M.S. (2007) Zscan4: a novel gene expressed exclusively in late 2-cell embryos and embryonic stem cells. *Dev. Biol.*, **307**, 539–550.
14. Kanka, J. (2003) Gene expression and chromatin structure in the pre-implantation embryo. *Theriogenology*, **59**, 3–19.
15. Schultz, R.M. and Worrad, D.M. (1995) Role of chromatin structure in zygotic gene activation in the mammalian embryo. *Semin. Cell Biol.*, **6**, 201–208.
16. Thompson, E.M., Legouy, E. and Renard, J.P. (1998) Mouse embryos do not wait for the MBT: chromatin and RNA polymerase remodeling in genome activation at the onset of development. *Dev. Genet.*, **22**, 31–42.
17. Stros, M., Launholt, D. and Grasser, K.D. (2007) The HMG-box: a versatile protein domain occurring in a wide variety of DNA-binding proteins. *Cell. Mol. Life Sci.*, **64**, 2590–2606.
18. Zhang, Q. and Wang, Y. (2008) High mobility group proteins and their post-translational modifications. *Biochim. Biophys. Acta*, **1784**, 1159–1166.
19. Schultz, J., Milpetz, F., Bork, P. and Ponting, C.P. (1998) SMART, a simple modular architecture research tool: identification of signaling domains. *Proc. Natl Acad. Sci. USA*, **95**, 5857–5864.
20. Mamo, S., Gal, A.B., Bodo, S. and Dinnyes, A. (2007) Quantitative evaluation and selection of reference genes in mouse oocytes and embryos cultured in vivo and in vitro. *BMC Dev. Biol.*, **7**, 14.
21. Hock, R., Furusawa, T., Ueda, T. and Bustin, M. (2007) HMG chromosomal proteins in development and disease. *Trends Cell Biol.*, **17**, 72–79.
22. Svarcova, O., Dinnyes, A., Polgar, Z., Bodo, S., Adorjan, M., Meng, Q. and Maddox-Hyttel, P. (2009) Nucleolar re-activation is delayed in mouse embryos cloned from two different cell lines. *Mol. Reprod. Dev.*, **76**, 132–141.
23. Sanij, E., Poortinga, G., Sharkey, K., Hung, S., Holloway, T.P., Quin, J., Robb, E., Wong, L.H., Thomas, W.G., Stefanovsky, V. *et al.* (2008) UBF levels determine the number of active ribosomal RNA genes in mammals. *J. Cell Biol.*, **183**, 1259–1274.
24. Stefanovsky, V.Y., Pelletier, G., Hannan, R., Gagnon-Kugler, T., Rothblum, L.I., Moss, T., Bazett-Jones, D.P. and Crane-Robinson, C. (2001) An immediate response of ribosomal transcription to growth factor stimulation in mammals is mediated by ERK phosphorylation of UBF DNA looping in the RNA polymerase I enhancesome is the result of non-cooperative in-phase bending by two UBF molecules. *Mol. Cell.*, **8**, 1063–1073.
25. Stefanovsky, V.Y., Pelletier, G., Bazett-Jones, D.P., Crane-Robinson, C. and Moss, T. (2001) DNA looping in the RNA polymerase I enhancesome is the result of non-cooperative in-phase bending by two UBF molecules. *Nucleic Acids Res.*, **29**, 3241–3247.
26. Mais, C., Wright, J.E., Prieto, J.L., Raggett, S.L. and McStay, B. (2005) UBF-binding site arrays form pseudo-NORs and sequester the RNA polymerase I transcription machinery. *Genes Dev.*, **19**, 50–64.
27. Falciola, L., Spada, F., Calogero, S., Langst, G., Voit, R., Grummt, I. and Bianchi, M.E. (1997) High mobility group 1 protein is not stably associated with the chromosomes of somatic cells. *J. Cell Biol.*, **137**, 19–26.
28. Bonaldi, T., Talamo, F., Scaffidi, P., Ferrera, D., Porto, A., Bachi, A., Rubartelli, A., Agresti, A. and Bianchi, M.E. (2003) Monocytic cells hyperacetylate chromatin protein HMGB1 to redirect it towards secretion. *EMBO J.*, **22**, 5551–5560.
29. Wang, H., Bloom, O., Zhang, M., Vishnubhakat, J.M., Ombrellino, M., Che, J., Frazier, A., Yang, H., Ivanova, S., Borovikova, L. *et al.* (1999) HMG-1 as a late mediator of endotoxin lethality in mice. *Science*, **285**, 248–251.
30. Cui, X.S., Shen, X.H. and Kim, N.H. (2008) High mobility group box 1 (HMGB1) is implicated in preimplantation embryo development in the mouse. *Mol. Reprod. Dev.*, **75**, 1290–1299.
31. Payer, B., Saitou, M., Barton, S.C., Thresher, R., Dixon, J.P., Zahn, D., Colledge, W.H., Carlton, M.B., Nakano, T. and Surani, M.A. (2003) Stella is a maternal effect gene required for normal early development in mice. *Curr. Biol.*, **13**, 2110–2117.
32. Gurtu, V.E., Verma, S., Grossmann, A.H., Liskay, R.M., Skarnes, W.C. and Baker, S.M. (2002) Maternal effect for DNA mismatch repair in the mouse. *Genetics*, **160**, 271–277.
33. Hock, R., Scheer, U. and Bustin, M. (1998) Chromosomal proteins HMG-14 and HMG-17 are released from mitotic chromosomes and imported into the nucleus by active transport. *J. Cell Biol.*, **143**, 1427–1436.
34. Mitsui, K., Tokuzawa, Y., Itoh, H., Segawa, K., Murakami, M., Takahashi, K., Maruyama, M., Maeda, M. and Yamanaka, S. (2003) The homeoprotein Nanog is required for maintenance of pluripotency in mouse epiblast and ES cells. *Cell*, **113**, 631–642.
35. Kim, J.B., Zaehres, H., Wu, G., Gentile, L., Ko, K., Sebastiano, V., Arauzo-Bravo, M.J., Ruau, D., Han, D.W., Zenke, M. *et al.* (2008)

Pluripotent stem cells induced from adult neural stem cells by reprogramming with two factors. *Nature*, **454**, 646–650.
36. Levine, A.J. and Brivanlou, A.H. (2006) GDF3, a BMP inhibitor, regulates cell fate in stem cells and early embryos. *Development*, **133**, 209–216.
37. Takahashi, K., Mitsui, K. and Yamanaka, S. (2003) Role of ERas in promoting tumour-like properties in mouse embryonic stem cells. *Nature*, **423**, 541–545.
38. Nimura, K., Ishida, C., Koriyama, H., Hata, K., Yamanaka, S., Li, E., Ura, K. and Kaneda, Y. (2006) Dnmt3a2 targets endogenous Dnmt3L to ES cell chromatin and induces regional DNA methylation. *Genes Cells*, **11**, 1225–1237.
39. Arima, T., Hata, K., Tanaka, S., Kusumi, M., Li, E., Kato, K., Shiota, K., Sasaki, H. and Wake, N. (2006) Loss of the maternal imprint in Dnmt3Lmat-/- mice leads to a differentiation defect in the extraembryonic tissue. *Dev. Biol.*, **297**, 361–373.
40. Pan, H., O'Brien, M.J., Wigglesworth, K., Eppig, J.J. and Schultz, R.M. (2005) Transcript profiling during mouse oocyte development and the effect of gonadotropin priming and development in vitro. *Dev. Biol.*, **286**, 493–506.
41. Saitou, N. and Nei, M. (1987) The neighbor-joining method: a new method for reconstructing phylogenetic trees. *Mol. Biol. Evol.*, **4**, 406–425.
42. Nagy, A., Gertsenstein, M., Vintersten, K. and Behringer, R. (2003) *Manipulating the Mouse Embryo: A Laboratory Manual.*, 3rd edn. Cold Spring Harbor Laboratory.
43. Hamatani, T., Falco, G., Carter, M.G., Akutsu, H., Stagg, C.A., Sharov, A.A., Dudekula, D.B., VanBuren, V. and Ko, M.S. (2004) Age-associated alteration of gene expression patterns in mouse oocytes. *Hum. Mol. Genet.*, **13**, 2263–2278.
44. Falco, G., Stanghellini, I. and Ko, M.S. (2006) Use of Chuk as an internal standard suitable for quantitative RT-PCR in mouse preimplantation embryos. *Reprod. Biomed. Online*, **13**, 394–403.

# Growth Differentiation Factor 9 Promotes Rat Preantral Follicle Growth by Up-Regulating Follicular Androgen Biosynthesis

Makoto Orisaka, Jin-Yi Jiang, Sanae Orisaka, Fumikazu Kotsuji, and Benjamin K. Tsang

Reproductive Biology Unit and Division of Reproductive Medicine (M.O., J.-Y.J., S.O., B.K.T.), Departments of Obstetrics and Gynaecology and Cellular and Molecular Medicine, University of Ottawa, Ottawa, Ontario, Canada K1H 8L6; Chronic Disease Program, Ottawa Health Research Institute, The Ottawa Hospital (Civic Campus), Ottawa, Ontario, Canada K1Y 4E9; and Department of Obstetrics and Gynecology (M.O., S.O., F.K.), University of Fukui, Matsuoka, Fukui, Japan 910-1193

The transition from preantral to early antral stage is the penultimate stage of ovarian follicular development in terms of gonadotropin dependence and follicle destiny. Although oocyte-somatic cell communication is important in early follicular development, our knowledge of the precise role of the oocyte-derived growth differentiation factor (GDF)-9 during preantral follicle growth is incomplete. We examined whether and by what means oocyte-derived GDF-9 controls follicular development and steroidogenesis during the preantral to early antral transition, by a combination of *in vitro* gene manipulation (*i.e.* intraoocyte injection of GDF-9 antisense oligos) and preantral follicle culture. Intraoocyte injection of GDF-9 antisense suppressed rat preantral follicle growth *in vitro*, whereas GDF-9 enhanced follicular development. GDF-9 augmented testosterone production in preantral follicles. GDF-9 antisense suppressed androgen production and CYP17A1 mRNA expression in cultured follicles, a response attenuated by exogenous GDF-9. The nonaromatizable androgen 5α-dihydrotestosterone rescued the follicular growth arrest caused by GDF-9 down-regulation. The specific androgen receptor antagonist flutamide suppressed GDF-9-induced preantral follicle growth *in vitro*. The data suggest that GDF-9 plays an important role in promoting preantral follicle growth by up-regulating follicular androgen biosynthesis. GDF-9 is essential for CYP17A1 expression during follicular development from the preantral to the early antral stage. (***Endocrinology*** **150: 2740–2748, 2009)**

The ovarian follicle, consisting of an oocyte surrounded by granulosa and thecal cells, represents the basic functional unit of the ovary. Follicular growth can be classified into three phases according to their developmental stage and gonadotropin dependence (1): 1) follicular growth through primordial, primary, and secondary stages (gonadotropin independent phase); 2) transition from preantral to early antral stage (gonadotropin responsive phase), and the growth of these follicles is primarily controlled by intraovarian regulators and does not require gonadotropins (2), although it is also stimulated by the presence of FSH (1); and 3) continual growth beyond the early antral stage (gonadotropin dependent phase), which includes follicle recruitment, selection, and ovulation (3). The preantral-early antral transition is the penultimate stage of development in terms of gonadotropin dependence and follicle destiny [growth *vs.* atresia (4)].

Oocyte-somatic cell communication plays a critical role in folliculogenesis, including activation of resting follicles, early growth, and terminal differentiation (5, 6). Growth differentiation factor (GDF)-9 is an oocyte-derived factor and a member of the TGF-β superfamily, which includes TGF-β, activin, and bone morphogenetic proteins (BMPs) (7, 8). GDF-9 is expressed in the mammalian oocyte throughout follicular development (9, 10). Deletion of the GDF-9 gene in mice blocked folliculogenesis at the primary stage, demonstrating the importance of this growth factor in early follicular development (11). GDF-9 stimulates granulosa cell mitosis (12) and suppresses granulosa cell apoptosis (4) in rat small antral follicles. GDF-9 has been shown to

ISSN Print 0013-7227 ISSN Online 1945-7170
Printed in U.S.A.

doi: 10.1210/en.2008-1536 Received November 5, 2008. Accepted January 30, 2009.
First Published Online February 12, 2009

Abbreviations: AR, Androgen receptor; BMP, bone morphogenetic protein; CTL, control; DHT, 5α-dihydrotestosterone; EIA, enzyme immunoassay; GDF, growth differentiation factor; MO, morpholino antisense oligonucleotide; Smad, Sma- and Mad-related protein.

enhance rat preantral follicle growth (13), although its precise mechanism(s) is obscure.

Ovarian steroids, which include progesterone, androgen, and estrogen, act via specific nuclear receptors and are essential for normal folliculogenesis and ovulation (14). Progesterone receptor (15) or estrogen receptor (16) null mice are infertile, and androgen receptor (AR) null mice culminate in reduced fertility and premature ovarian failure (17), indicating that these steroids are essential for reproductive function and fertility. Although the exact role of GDF-9 on follicular cell differentiation during the transition of the follicle from preantral to early antral stage is not clear, GDF-9 is known to stimulate basal estradiol synthesis and suppress FSH-induced progesterone and estradiol production in undifferentiated rat granulosa cells (12). The role of GDF-9 on thecal cell androgen production is less clear. Whereas Solovyeva *et al.* (18) showed that GDF-9 stimulates androstenedione production in rat theca-interstitial cell, Spicer *et al.* (19) reported that GDF-9 inhibits androstenedione production by bovine thecal cells from small antral follicles. Although GDF-9 promotes granulosa cell mitosis and preantral follicle growth, whether the latter response is mediated via follicular steroidogenesis is not known.

In the present studies, we hypothesized that oocyte-derived GDF-9 stimulates preantral follicle growth in part by up-regulating follicular steroidogenesis. We examined whether and by what means GDF-9 and FSH regulate follicular development and steroid production during preantral-early antral transition by a combination of *in vitro* gene manipulation and preantral follicle culture. We have demonstrated that GDF-9 promotes preantral follicle growth by stimulating follicular androgen biosynthesis.

## Materials and Methods

### Materials

All culture media and supplements were purchased from Life Technologies Inc. (Burlington, Ontario, Canada). Bovine insulin, human transferrin, ascorbic acid, sodium selenite anhydrous, L-glutamine, and agarose (low gelling temperature) were obtained from Sigma Chemical Co. (St. Louis, MO). Recombinant human FSH was obtained from the National Hormone and Peptide Program, Harbor-UCLA Medical Center (Torrance, CA). Morpholino antisense oligos (MOs) for control (CTL) and GDF-9 were purchased from Gene-Tools, LLC (Philomath, OR). Intracytoplasmic sperm injection micropipettes (no. MIC-35-30) were from Humagen (Charlottesville, VA). Goat antihuman GDF-9 antibody (C-18) and its blocking peptide as well as goat ImmunoCruz staining system were from Santa Cruz Biotechnology, Inc. (Santa Cruz, CA). Progesterone and testosterone enzyme immunoassay (EIA) kit were from R&D Systems, Inc. (Minneapolis, MN), whereas the estradiol EIA kit was from Calbiotech, Inc. (Spring Valley, CA). 5α-Dihydrotestosterone (DHT), estradiol, and flutamide, a specific AR antagonist, were from Sigma-Aldrich Co. (St. Louis, MO). RNeasy microkit and QuantiTect SYBR Green PCR kit were purchased from QIAGEN, Inc. (Mississauga, Ontario, Canada). Random decamer primers were from Ambion, Inc. (Austin, TX). PCR primers for CYP17A1, AR, and 18S rRNA were from Invitrogen Canada, Inc. (Burlington, Ontario, Canada). Recombinant rat GDF-9 was generously provided by Dr. Aaron J. W. Hsueh (Stanford University School of Medicine, Stanford, CA).

### Preantral follicle isolation and culture

All animal procedures were carried out in accordance with the guidelines of the Canadian Council on Animal Care and approved by the Ottawa Health Research Institute Animal Care Committee. Female Sprague Dawley rats were obtained from Charles River Canada (Montréal, Québec, Canada) and maintained under standard conditions.

Large preantral follicles (diameter, 150–170 μM) were isolated from 14-d-old rats in Leibowitz L-15 medium with BSA (0.1%, wt/vol) at d 0, using 28.5-gauge needles (Becton Dickinson and Co., Franklin Lakes, NJ). Only round follicles with intact basement membrane and thecal layer were selected for the present studies. Follicles were cultured individually in a 96-well plate (Sarstedt, Inc., Newton, NC; no. 83.1837.50) in 100 μl of α-MEM supplemented with HEPES (10 mM), BSA (0.1%, wt/vol), bovine insulin (5 μg/ml), transferrin (2 μg/ml), ascorbic acid (25 μg/ml), sodium selenite anhydrous (2 ng/ml), L-glutamine (3 mM), sodium pyruvate (100 μg/ml), streptomycin (100 μg/ml), and penicillin (100 U/ml), with or without 100 ng/ml of GDF-9 and different concentrations of FSH (10 or 100 ng/ml). Preliminary data indicated that 100 ng/ml of GDF-9 or 10 ng/ml of FSH are the minimal effective concentrations for inducing a significant increase in preantral follicle growth in our culture system. Follicular diameter was measured daily as the average of distance between the outer edges of the basement membrane in two perpendicular planes and results were expressed as change in follicular volume. The percentage change of follicular volume on day n of culture is defined as the volume difference between day n and d 0 (the day of isolation) expressed as a percentage of the volume at d 0. The culture medium was changed every other day, and the spent media were kept at −20 C for steroid assays.

### Intraoocyte injection of MO oligonucleotides in preantral follicles

Expression of MOs is effective in suppressing translation of target genes in zebrafish (20) and *Xenopus* (21) embryos. As described previously (4), to assess the role of GDF-9 on follicular development and steroidogenesis during preantral-early antral transition, GDF-9 content in the cultured follicles was manipulated by intraoocyte microinjection of GDF-9 MO. The GDF-9 MO sequence was designed based on its rat cDNA sequence (5′-ACAGGAATCTGCTGGGAAATGCCAT-3′, not homologous with BMP-15/GDF-9B cDNA). The standard CTL MO sequence (5′-CCTCTTACCTCAGTTACAATTTATA-3′) designed by Gene-Tools was not expressed in the follicles and caused no phenotype on follicular growth and steroidogenesis in the injected/cultured preantral follicles. The MOs were fluorescent tagged with Lissamine, which was visible by fluorescence microscopy. Large preantral follicles isolated from 14-d-old rats were cultured individually in a 96-well plate without GDF-9 or FSH. After 16–24 h, only the follicles (diameter 150–170 μM) with intact basement membrane and thecal layer were selected for the microinjection. CTL MO or GDF-9 MO (10 μM) was injected into the oocyte of the preantral follicles at d 0. The volume of MO injected (3 pl) was less than 5% (vol/vol) of the oocyte volume. Successful injection was confirmed by visualization of fluorescence (Lissamine tag). At d 1 (*i.e.* 24 h after intraoocyte injection), the oocyte morphology was evaluated microscopically, and only follicles with morphologically intact oocytes were cultured with or without GDF-9 (100 ng/ml) and FSH (10 ng/ml) for another 3 d (d 1 to d 4). Follicular diameter was measured daily and the culture medium was changed every other day. The percentage change of follicular volume on day n of culture is defined as the volume difference between day n and d 0 (the day of microinjection) expressed as a percentage of the volume at d 0. At the end of the culture period, follicles were fixed and embedded, as described previously (7), for GDF-9 immunohistochemistry. The spent media were kept at −20 C for steroid assays. The follicle were also pooled and kept at −80 C for real-time PCR analyses.

To assess the role of androgen and estrogen on GDF-9-induced preantral follicle growth, the CTL MO- and GDF-9 MO-injected (at d 0) follicles were cultured with different concentrations of DHT (0 to 10 μM) or estradiol (0 to 10 μM) for 3 d (d 1 to d 4). Moreover, to ascertain the

direct effect of androgens, the CTL MO- and GDF-9 MO-injected follicles were preincubated for 1 h (at d 1) with different concentration of the AR antagonist flutamide (0–10 $\mu$M) before the addition of GDF-9 (100 ng/ml) and cultured for another 3 d (d 1 to d 4). Follicular diameter was measured daily, and results were expressed as change in follicular volume.

### GDF-9 immunohistochemistry

The GDF-9 content in the injected/cultured follicles was examined by immunohistochemistry, according to the previous protocol (7). The intensity of GDF-9 immunostain in 10 oocytes for each group at d 4 of culture was semiquantified using a relative scale: 0, 1, and 2 for no (see Fig. 2Ad), weak, and strong (see Fig. 2Ac) staining, respectively.

### Steroid assays

The levels of progesterone, testosterone, and estradiol in the spent media were measured using the respective EIA kits (as described in *Materials and Methods*) according to the manufacturer's instructions. The intraassay coefficient of variation for progesterone, testosterone, and estradiol were 6.0, 9.5, and 10.9%, respectively, whereas the interassay coefficient of variation for progesterone, testosterone, and estradiol was 5.9, 11.7, and 12.5%, respectively. The sensitivity of the progesterone, testosterone, and estradiol assays was 9, 6, and 10 pg/ml, respectively.

### Real-time PCR analysis of CYP17A1 and AR expression

Total RNAs from three MO-injected follicles (pooled from the same experiment group) were extracted, using RNeasy microkit according to manufacturer's instructions. Real-time quantitative PCR analysis for CYP17A1 and AR was performed on the follicular cDNAs, using a LightCycler 2.0 system (Roche Diagnostic Canada, Laval, Quebec, Canada). The primers of CYP17A1 used for amplification were a 5′-forward primer (5′-ACTGAGGGTATCGTGGATGC-3′) and a 3′-reverse primer (5′-TC GAACTTCTCCCTGCACTT-3′), whereas those of AR were a 5′-forward primer (5′-GGGTGACTTCTCTGCCTCTG-3′) and a 3′-reverse primer (5′-AAACGTGGTCCCTGGTACTG-3′). The transcript levels of CYP17A1 and AR were normalized against those of 18S rRNA (5′-forward primer; 5′-CGCGGTTCTATTTTGTTGGT-3′, 3′-reverse primer; 5′-AGTCGGCATCGTTTATGGTC-3′). Amplification reaction was then performed using the QuantiTect SYBR Green PCR kit (QIAGEN). The thermal cycling conditions comprised an initial denaturation step at 95 C for 15 min and 50 cycles (CYP17A1) or 40 cycles (AR and 18S rRNA) at 95 C for 15 sec, 56 C for 20 sec, and 72 C for 30 sec. The levels of CYP17A1 and AR mRNA were expressed as a ratio to 18S rRNA values.

### Statistical analysis

Results are presented as means ± SEM of at least three independent experiments. All data were subjected to one- or two-way (repeated measure) ANOVA, except unpaired *t* test for immunostaining intensity of GDF-9 in oocytes (Prism 4.0 and InStat 3.0 statistical software; GraphPad Software, Inc., San Diego, CA). Differences between experimental groups were determined by the Tukey or Bonferroni posttest. Statistical significance was inferred at $P < 0.05$.

## Results

### Effects of GDF-9 and FSH on preantral follicular growth and steroidogenesis *in vitro*

To examine the effect of GDF-9 and FSH on preantral follicular growth, rat large preantral follicles were cultured with or without 100 ng/ml of GDF-9 and different concentrations of FSH (10 or 100 ng/ml) for 4 d. Preantral follicles cultured in the absence of GDF-9 and FSH exhibited minimal growth (Fig. 1A).

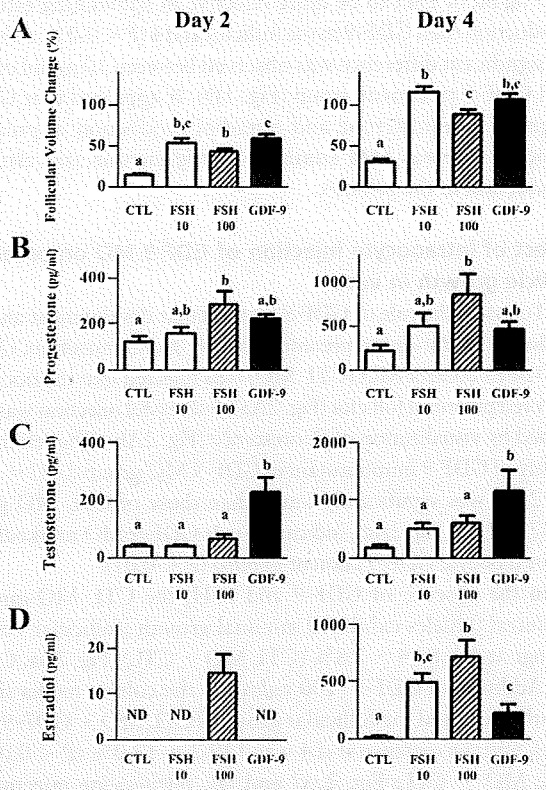


**FIG. 1.** Effects of GDF-9 and FSH on preantral follicular growth and steroidogenesis *in vitro*. A, Rat preantral follicles (150–170 $\mu$M in diameter) were cultured for 4 d with or without GDF-9 (100 ng/ml) and different concentrations of FSH [10 ng/ml ($FSH_{10}$) or 100 ng/ml ($FSH_{100}$)]. CTL, Preantral follicles were cultured in the absence of GDF-9 and FSH. Follicular diameter was measured daily and results were expressed as change in follicular volume. The percentage change of follicular volume on day n of culture is defined as the volume difference between day n and d 0 (the day of isolation) expressed as a percentage of the volume at d 0. Results are presented as means ± SEM of a total of 40 follicles from six to eight independent experiments. ND, Not detected. *Bars with different superscripts* are significantly different at $P < 0.05$. Note that GDF-9 and FSH stimulated preantral follicular growth (A). B–D, Concentrations of progesterone (B), testosterone (C), and estradiol (D) in the spent media on d 2 and d 4 were measured. Note that GDF-9 augmented testosterone and estradiol production in preantral follicles, whereas FSH stimulated progesterone and estradiol production in the follicles.

An increase in follicular volume was seen as early as 2 d after treatment with either GDF-9 or FSH ($P < 0.05$ *vs.* CTL). Addition of GDF-9 to the culture media significantly increased follicular growth at d 4 ($P < 0.01$ *vs.* CTL; Fig. 1A). Because10 ng/ml of FSH appeared more effective on preantral follicle growth than 100 ng/ml of FSH at d 4 ($P < 0.01$), 10 ng/ml of FSH was used for the later microinjection studies.

To determine the influence of GDF-9 and FSH on follicular steroidogenesis during preantral follicle growth, the concentrations of progesterone, testosterone, and estradiol in the spent media were determined. Although 100 ng/ml of FSH augmented progesterone production in preantral follicles ($P < 0.05$ *vs.* CTL), neither 10 ng/ml of FSH nor GDF-9 significantly influences progesterone biosynthesis (Fig. 1B). Treatment with GDF-9 stimulated testosterone production in the preantral follicles ($P < 0.01$ *vs.* CTL), whereas FSH did not significantly affect testosterone level in the follicles (Fig. 1C). GDF-9 and FSH augmented estrogen production in the preantral follicles. We found

100 ng/ml of FSH to be more effective in stimulating estradiol production than GDF-9 in the follicles at d 4 ($P < 0.01$), although no significant difference was observed between 10 ng/ml of FSH and GDF-9 treatment group (Fig. 1D). It appeared that GDF-9 augmented testosterone and estradiol production in preantral follicles, whereas FSH stimulated progesterone and estradiol production in the follicles.

### Effect of intraoocyte injection of GDF-9 MO on preantral follicle growth *in vitro*

To assess the role of GDF-9 on follicular development and steroidogenesis during the preantral to early antral transition, GDF-9 MO or its control MO (CTL MO) was injected into the oocyte of cultured preantral follicles (Fig. 2Aa). Successful injection was confirmed by visualization of fluorescence (Fig. 2Ab). The relative intensity of GDF-9 immunostain in GDF-9 MO group (0.33 ± 0.21; Fig 2Ad) was significantly lower than those of CTL MO group (1.67 ± 0.21; Fig. 2Ac), indicating that GDF-9 MO markedly decreased oocyte GDF-9 content *in vitro* ($P < 0.01$).

In the absence of GDF-9 and FSH, the CTL MO-injected preantral follicles exhibited minimal growth [follicular volume change at d 4: 60.4 ± 7.8% (CTL MO + CTL); Fig. 2Ba, C, and D]. Addition of GDF-9 (100 ng/ml) to the culture media significantly increased the follicular growth (CTL MO + GDF-9; Fig. 2Bb), and the increase at d 4 was 129.2 ± 13.0% ($P < 0.01$ *vs.* CTL MO + CTL; Fig. 2, C and D). Intraoocyte injection of GDF-9 MO suppressed basal preantral follicle growth during 4-d culture period (Fig. 2Bc). Whereas basal follicular volume in the CTL MO + CTL group was significantly increased by d 4 ($P < 0.05$), a decrease was noted in the GDF-9 MO + CTL group (−19.8 ± 5.1%), resulting in a significant difference between the two experimental groups ($P < 0.01$; Fig. 2, C and D). The effect of GDF-9 MO appeared to be specific to GDF-9 because the addition of GDF-9 to the culture media prevented the follicular growth arrest caused by GDF-9 MO (Fig. 2Bd). No significant difference in the change in follicular volume was observed between the CTL MO + CTL and the GDF-9 MO + GDF-9 group ($P > 0.05$; Fig. 2, C and D).

FSH (10 ng/ml) stimulated preantral follicle growth ($P < 0.05$, CTL MO + FSH *vs.* CTL MO + CTL; Fig. 2D). In the presence of FSH, GDF-9 down-regulation also suppressed follicular growth ($P < 0.01$, GDF-9 MO + FSH *vs.* CTL MO + FSH).

### Effect of intraoocyte injection of GDF-9 MO on steroidogenesis in preantral follicles *in vitro*

Although FSH augmented progesterone production in preantral follicles ($P < 0.01$, CTL MO + FSH *vs.* CTL MO + CTL), neither the addition of GDF-9 nor GDF-9 down-regulation significantly influence progesterone biosynthesis irrespective of the presence of FSH (Fig. 3A). There was no significant difference in the progesterone concentration between the CTL MO + CTL, CTL MO + GDF-9, GDF-9 MO + CTL, and GDF-9 MO + GDF-9 group ($P > 0.05$).

Treatment with GDF-9 stimulated testosterone production in the follicles injected with CTL MO [550.3 ± 108.5 pg/ml (CTL MO + GDF-9) *vs.* 268.6 ± 78.0 pg/ml (CTL MO + CTL), $P < 0.05$; . 3B]. GDF-9 MO markedly decreased androgen biosynthesis [14.1 ± 5.7 pg/ml (GDF-9 MO + CTL), $P < 0.05$ *vs.* CTL MO + CTL], a response attenuated by exogenous GDF-9 [475.9 ± 110.5 pg/ml (GDF-9 MO + GDF-9), $P < 0.01$ *vs.* GDF-9 MO + CTL]. The amount of testosterone in GDF-9 MO + GDF-9 was not different from those in CTL MO + CTL ($P > 0.05$; Fig. 3B). FSH did not affect testosterone level in the CTL

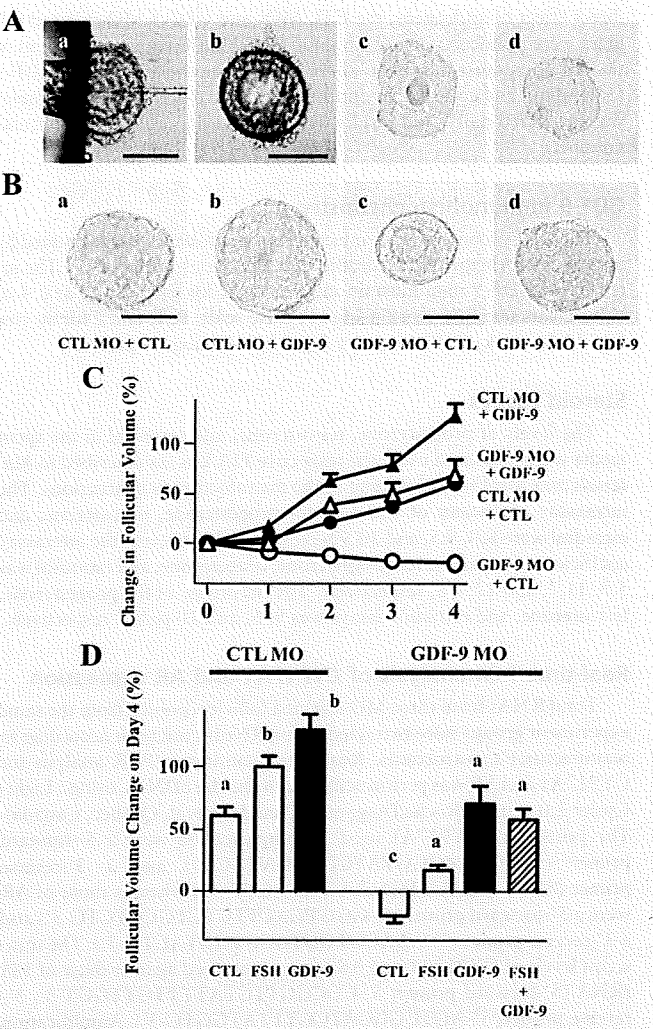


FIG. 2. Intraoocyte injection of CTL/GDF-9 MO in cultured preantral follicles and the influence of GDF-9 down-regulation on follicular growth *in vitro*. A, a and b, Intraoocyte injection of CTL/GDF-9 MO; c and d, GDF-9 expression (immunohistochemistry) in the CTL MO- (c) and GDF-9 MO-injected (d) follicles on d 4. Note that oocytes injected with GDF-9 MO exhibited significantly lower GDF-9 immunostain intensity compared with those with CTL MO. B, A representative image on d 4 is shown for each treatment group: a, CTL MO + CTL, b, CTL MO + GDF-9; c, GDF-9 MO + CTL, and d, GDF-9 MO + GDF-9, respectively. *Scale bar*, 100 μM. C and D, Effect of GDF-9 down-regulation on preantral follicle growth *in vitro*. CTL MO or GDF-9 MO was injected into the oocyte of the rat preantral follicles at d 0. At d 1, the follicles (diameter, 150–170 μm) were treated with or without GDF-9 (100 ng/ml) and FSH (10 ng/ml) and cultured for another 3 d (d 1–4). CTL, Preantral follicles cultured in the absence of GDF-9 and FSH. The percentage change of follicular volume on day n of culture is defined as the volume difference between day n and d 0 (the day of microinjection) expressed as a percentage of the volume at d 0. Results represent the means ± SEM of a total of 20 follicles from four or five independent experiments. *Bars with different superscripts* are significantly different at $P < 0.05$. Note that GDF-9 stimulated preantral follicle growth during a 4-d culture period. Although GDF-9 MO injection suppressed follicular growth, addition of GDF-9 to the culture media prevented the growth arrest induced by GDF-9 antisense on d 4.

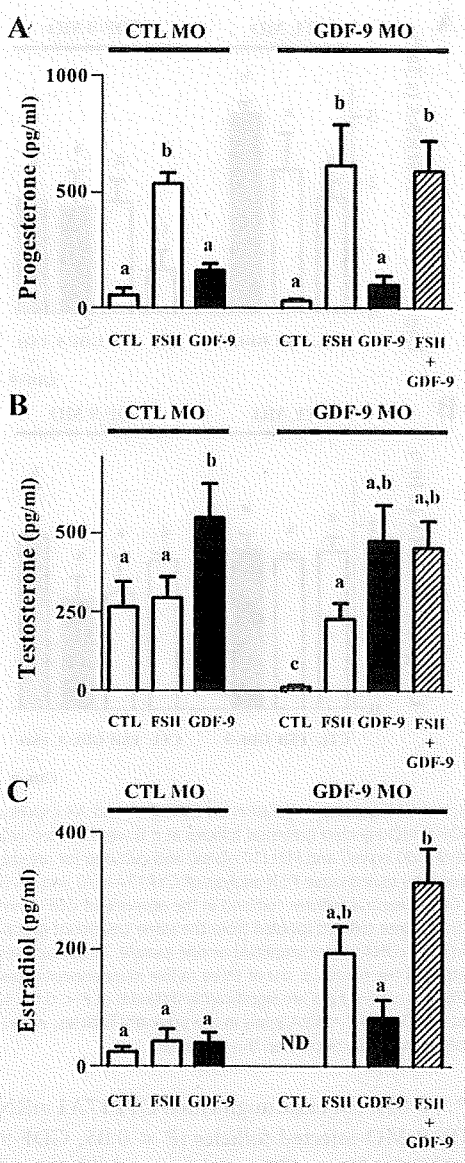


**FIG. 3.** Effect of intraoocyte injection of GDF-9 MO on steroidogenesis by preantral follicle *in vitro*. CTL/GDF-9 MO-injected preantral follicles at d 0 were treated with or without GDF-9 (100 ng/ml) and FSH (10 ng/ml) and cultured for another 3 d (d 1–4). CTL, Preantral follicles cultured in the absence of GDF-9 and FSH. Concentrations of progesterone (A), testosterone (B), and estradiol (C) in the spent media on d 4 were measured. Data are the mean ± SEM of a total of 20 follicles from four or five independent experiments. ND, Not detected. *Bars with different superscripts* are significantly different at $P < 0.05$. Note that GDF-9 MO markedly decreased androgen biosynthesis, although this response was attenuated by exogenous GDF-9.

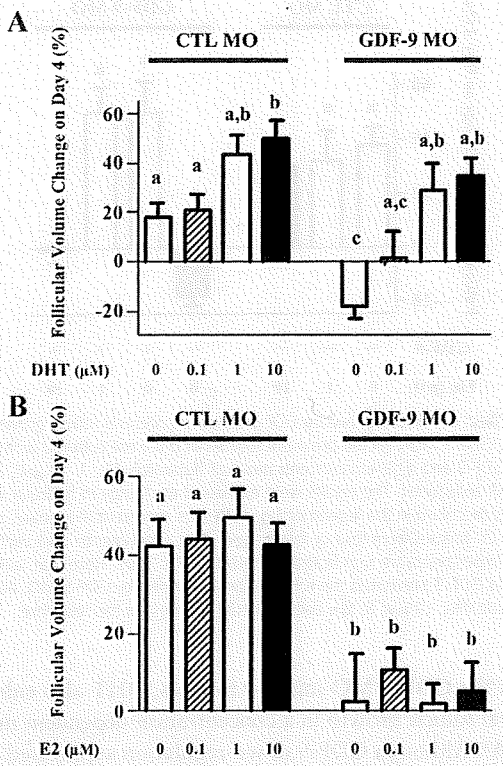


**FIG. 4.** Effect of DHT and estradiol on preantral follicle growth arrest induced by GDF-9 MO *in vitro*. CTL/GDF-9 MO-injected preantral follicles at d 0 were cultured with different concentrations of DHT (A; 0–10 μM), a nonaromatizable androgen, or estradiol (E2; B; 0–10 μM). The percentage change of follicular volume on d 4 of culture is defined as the volume difference between d 4 and d 0 (the day of microinjection) expressed as a percentage of the volume at d 0. Results represent the means ± SEM of a total of 20 follicles from four or five independent experiments. *Bars with different superscripts* are significantly different at $P < 0.05$. Note that the addition of DHT, not estradiol, to the culture media prevented the growth arrest induced by GDF-9 antisense on d 4.

MO-injected follicles ($P > 0.05$, CTL MO + FSH *vs.* CTL MO + CTL) but significantly suppressed GDF-9 MO-induced testosterone down-regulation ($P < 0.05$, GDF-9 MO + FSH *vs.* GDF-9 MO + CTL). GDF-9 appeared to be more effective in stimulating androgen production than FSH in the CTL MO-injected follicles [550.3 ± 108.5 pg/ml (CTL MO + GDF-9) *vs.* 293.3 ± 67.5 pg/ml (CTL MO + FSH), $P < 0.05$], although no significant difference was observed between the GDF-9 MO + GDF-9 and the GDF-9 MO + FSH group.

Although treatment with GDF-9 and FSH did not alter estradiol production in the follicles injected with CTL MO (Fig. 3C), GDF-9 MO markedly decreased estradiol production [< 10 pg/ml (GDF-9 MO + CTL) *vs.* 20.1 ± 7.3 pg/ml (CTL MO + CTL)]. In the GDF-9 MO-injected follicles, addition of GDF-9 into the culture media increased estradiol production [< 10 pg/ml (GDF-9 MO + CTL) *vs.* 84.2 ± 29.4 pg/ml (GDF-9 MO + GDF-9)]. FSH also augmented estradiol production in the GDF-9 MO-injected follicles irrespective of the presence of GDF-9 ($P < 0.01$).

Based on the results of Figs. 1 and 3, GDF-9 appeared to preferentially stimulate the production of testosterone rather than estradiol in the follicles during preantral to early antral transition.

## Androgen action is involved in GDF-9-induced preantral follicle growth *in vitro*

To determine whether and how androgen modulates GDF-9-induced preantral follicles *in vitro*, the CTL MO- and GDF-9 MO-injected follicles were cultured with different concentrations of DHT (0–10 μM), a nonaromatizable androgen. DHT augmented the CTL-MO injected follicular growth in a concentration-dependent manner ($P < 0.05$; Fig. 4A). Ten micromoles of DHT was the most effective concentration in inducing a significant increase in preantral follicle growth in our culture sys-

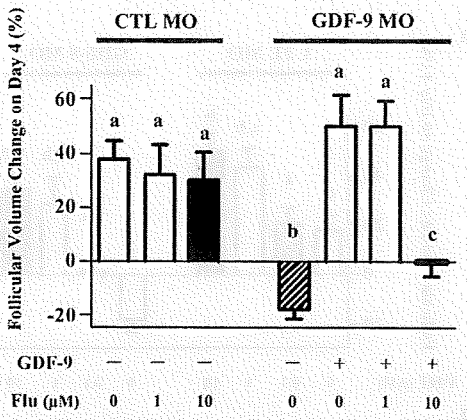


**FIG. 5.** Effect of AR antagonist on GDF-9-induced preantral follicle growth *in vitro*. CTL/GDF-9 MO-injected preantral follicles at d 0 were cultured with or without GDF-9 and different concentrations of flutamide (Flu; 1–10 μM), a specific AR antagonist. The results were expressed as change in follicular volume on d 4, as described in the legend of Fig. 4. Results represent the means ± SEM of a total of 20 follicles from four or five independent experiments. *Bars with different superscripts* are significantly different at $P < 0.05$. Note that, although exogenous GDF-9 prevented the follicular growth arrest by GDF-9 MO, addition of flutamide (Flu; 10 μM) to the culture media suppressed this response.

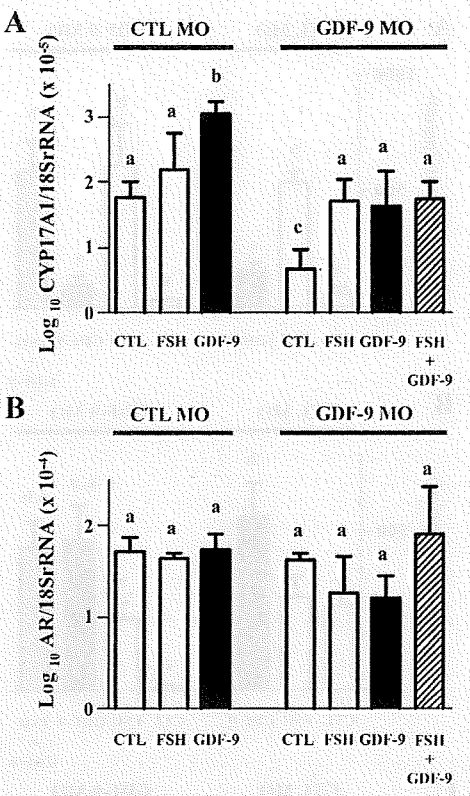


**FIG. 6.** Effect of GDF-9 down-regulation on CYP17A1 and AR expression *in vitro*. CTL/GDF-9 MO-injected preantral follicles at d 0 were treated with or without GDF-9 (100 ng/ml) and FSH (10 ng/ml) and cultured for another 3 d (d 1–4), and real-time quantitative PCR analysis of CYP17A1 (A) and AR (B) was performed. CTL, Preantral follicles cultured in the absence of GDF-9 and FSH. Total RNAs from three follicles (pooled from the same treatment group) were extracted, and the cDNAs were amplified as one sample. Results are represented as the logarithm of the means ± SEM of three to five independent experiments. *Bars with different superscripts* are significantly different at $P < 0.05$. Note that GDF-9 increased CYP17A1 mRNA levels in the preantral follicles, whereas GDF-9 down-regulation markedly decreased this response.

tem. In the GDF-9 MO-injected follicles, DHT also enhanced preantral follicle growth in a concentration-dependent manner (Fig. 4A). Although GDF-9 down-regulation suppressed follicular growth ($P < 0.01$), the addition of 1 and 10 μM of DHT to the culture media prevented this response ($P < 0.01$). In contrast, treatment with estradiol (0–10 μM) did not alter the growth of CTL-MO or GDF-9-MO injected follicles (Fig. 4B).

Furthermore, to examine the role of androgen action in GDF-9-induced preantral follicle growth, the CTL MO- and GDF-9 MO-injected follicles were cultured with or without GDF-9 and with different concentrations of flutamide (0–10 μM), a specific AR antagonist. Although exogenous GDF-9 prevented the follicular growth arrest caused by GDF-9 MO ($P < 0.01$), addition of flutamide (10 μM) to the culture media suppressed this response ($P < 0.01$; Fig. 5). Flutamide did not alter the growth of the CTL MO-injected follicles ($P > 0.05$). These results demonstrated that the effects of androgen on the GDF-9-induced preantral follicle growth were not due to aromatization to estradiol, and were inhibited by an antagonist to the androgen receptor.

### GDF-9 is essential for the expression of follicular CYP17A1 mRNA *in vitro*

To determine by what means GDF-9 regulates follicular androgen action during this stage, real-time quantitative PCR analysis of CYP17A1 (mainly expressed in thecal cells) and AR (mainly expressed in granulosa cells) was performed on total RNAs from the MO-injected follicles. GDF-9, but not FSH, augmented CYP17A1 mRNA levels in the follicles injected with CTL-MO ($P < 0.05$, CTL MO + GDF-9 *vs.* CTL MO + CTL), whereas GDF-9 MO markedly decreased this response ($P < 0.05$, GDF-9 MO + CTL *vs.* CTL MO + CTL; Fig. 6A). The down-regulation of CYP17A1 transcript by GDF-9 MO was prevented by exogenous GDF-9 ($P < 0.05$, GDF-9 MO + GDF-9 *vs.* GDF-9 MO + CTL), and CYP17A1 mRNA abundance in GDF-9 MO + GDF-9 was not different from those in CTL MO + CTL ($P > 0.05$). FSH also augmented CYP17A1 mRNA levels in the GDF-9 MO-injected follicles ($P < 0.05$, GDF-9 MO + FSH *vs.* GDF-9 MO + CTL). Addition of GDF-9 or GDF-9 down-regulation did not affect AR mRNA expression in the preantral follicles (Fig. 6B). No significant difference in AR mRNA abundance was observed between the CTL MO + CTL, CTL MO + GDF-9, GDF-9 MO + CTL, and GDF-9 MO + GDF-9 group ($P > 0.05$).

## Discussion

Although oocyte-somatic cell communication is important in early follicular development, our knowledge of the precise role of the oocyte-derived factor GDF-9 during the preantral-early antral transition is incomplete. In the present study, we have shown for the first time that: 1) intraoocyte injection of GDF-9 MO antisense suppressed rat preantral follicle growth *in vitro*, whereas GDF-9 enhanced follicular development; 2) GDF-9 augmented testosterone production in preantral follicles; 3) GDF-9 MO suppressed androgen production and CYP17A1 mRNA expression in cultured follicles, a response attenuated by exogenous

GDF-9; 4) the nonaromatizable androgen DHT rescued the follicular growth arrest by GDF-9 down-regulation; and 5) the specific AR antagonist flutamide suppressed GDF-9-induced preantral follicle growth *in vitro*. These results suggest that GDF-9 controls ovarian follicular development from the preantral stage to early antral stage by up-regulating follicular androgen biosynthesis.

The exact role of GDF-9 on follicular differentiation during preantral-early antral transition is not clear (19). Nevertheless, it is possible that GDF-9 stimulates thecal cell recruitment, proliferation, and differentiation and induces the formation of thecal cell layer during this early stage of the follicular development. Ovaries from GDF-9 null mice exhibit a developmental block at the primary follicle stage, which is characterized by failed thecal layer formation in early follicles (22). GDF-9 is believed to be more important for the differentiation than the recruitment of thecal cell because the double-mutant (GDF-9 and inhibin-$\alpha$) mouse exhibits morphological thecal cells surrounding the preantral follicles without detectable selective thecal markers, CYP17A1 and LH receptor (23). GDF-9 treatment increases androgen production in cultured rat theca-interstitial cells (18) and promotes murine ovarian expression of the specific thecal cell marker CYP17A1 (22). A recent study also indicated that GDF-9 increases thecal cell number and DNA synthesis in thecal cells of small bovine follicles (19). In the present studies, we demonstrated that GDF-9 augments androgen production and CYP17A1 mRNA expression in the preantral follicles, whereas GDF-9 down-regulation suppressed this response, indicating that GDF-9 is involved in the thecal cell differentiation during preantral-early antral transition. Whether the increased follicular CYP17A1 content is a result of increased thecal cell number and/or CYP17 levels per cell remains to be elucidated.

Ovarian androgens, primarily androstenedione and testosterone, are produced by thecal cells and act via receptors (ARs) localized to granulosa cells, stromal cells, and oocytes (14). Inactivation of AR in female mice results in premature ovarian failure, indicating that normal folliculogenesis requires AR-mediated androgen action (17). AR expression is highest in granulosa cells of rat small preantral and early antral follicles (24), raising the possibility that androgens are important paracrine regulators of follicular growth during preantral to early antral transition. Although androgens have long been implicated as an inhibitor of antral follicular development (25, 26), recent evidence suggests that the effect of androgens on follicular growth is dependent on the stage of follicular development and that androgens also have a growth promoting role in early folliculogenesis. Administration of testosterone or DHT to adult rhesus monkeys significantly increased the number of preantral and small antral follicles as well as granulosa and thecal cell proliferation (27). *In vitro* studies have shown that androgens (*e.g.* testosterone, DHT, androstenedione) stimulate preantral follicle growth and granulosa cell mitosis in mice (28), the transition of primary follicle to secondary follicle in cattle (29), and follicular survival in humans (30). An AR antagonist, but not an aromatase inhibitor, inhibited this growth response, indicating that the conversion of androgens to estrogens was not responsible for the follicle growth (31). DHT has also been shown to enhance porcine granulosa cell proliferation by facilitating the action of GDF-9 *in vitro* (32). In the present study, the nonaromatizable androgen DHT, but not estradiol, rescued the follicular growth arrest by GDF-9 down-regulation. The specific AR antagonist flutamide suppressed GDF-9-induced preantral follicle growth *in vitro*. These findings suggest that androgens exert a direct stimulatory action on the follicular development, especially during the preantral-early antral stage transition.

Androgens enhance the FSH action in the follicles by increasing FSH receptor expression, FSH-induced granulosa cell aromatase activity and proliferation, and follicular growth (33). GDF-9 augments FSH-induced preantral follicle growth (4, 17), whereas GDF-9 down-regulation suppressed FSH-stimulated follicular development. Although GDF-9 is required for the expression of FSH receptor in rat preantral follicles (4), whether these growth responses are modulated through thecal androgen actions awaits further investigation.

Tetsuka *et al.* (24) reported that a gradient of AR immunostaining existed in large follicles of the rat ovary, with cumulus cells and antral granulosa cells strongly expressing more AR protein than do peripheral layers. Nevertheless, the present result suggests that GDF-9 is not the oocyte-secreted factor that influences AR expression in follicles because GDF-9 did not alter AR mRNA levels in the cultured preantral follicles.

Previous study showed that GDF-9 stimulates basal estradiol synthesis in rat undifferentiated granulosa cells but suppresses FSH-induced progesterone and estradiol production (12). Because granulosa cells often undergo luteinization in culture (34) and excess FSH induces premature granulosa cell differentiation *in vitro* (35), it is possible that some of the granulosa cell responses *in vitro* might be more related to a potential role for GDF-9 in inhibiting premature luteinization rather than to its effect on normal follicular function (13, 18). Nevertheless, the present studies indicate that GDF-9 stimulates preantral follicle production of estradiol, but not progesterone, although whether GDF-9 enhances the expression of aromatase in granulosa cells and/or increases the synthesis of androgen substrate for aromatization remains to be elucidated. In the GDF-9 MO-injected follicles, FSH stimulated progesterone and estradiol production in the preantral follicles irrespective of the presence of GDF-9, which might be related to the FSH-induced expression of steroidogenic acute regulatory (36), CYP11A1 (36), and CYP19A1 (37) genes in granulosa cells. Solovyeva *et al.* (18) reported that GDF-9 enhanced forskolin-stimulated androstenedione production in rat theca-interstitial cells, whereas Spicer *et al.* reported that GDF-9 inhibits LH and IGF1-induced steroidogenesis by bovine thecal cells (19). Whether thecal cells also undergo luteinization *in vitro* and GDF-9 modulates this process, is not known.

Although the present results suggest that GDF-9 controls preantral follicle growth by up-regulating thecal CYP17AI expression and androgen biosynthesis, whether the observed effect of GDF-9 is mediated through a direct action on thecal cells or indirectly on granulosa cells remains to be investigated. GDF-9 signals through a complex of type I (activin-like receptor kinase-5) and type II (BMP receptor type II) membrane serine/threonine kinase receptors (38), resulting in the phosphorylation